chemosensors

MDPI

Review

Laser-Scribed Graphene-Based Electrochemical Sensors: A Review

Wilson A. Ameku, Masoud Negahdary, Irlan S. Lima, Berlane G. Santos, Thawan G. Oliveira, Thiago R. L. C. Paixão and Lúcio Angnes *

Institute of Chemistry, Department of Fundamental Chemistry, University of São Paulo, São Paulo 05508-000, Brazil
* Correspondence: luangnes@iq.usp.br; Tel.: +55-11-3091-3828

Abstract: Laser scribing is a technique that converts carbon-rich precursors into 3D-graphene nanomaterial via direct, single-step, and maskless laser writing in environmental conditions and using a scalable approach. It allows simple, fast, and reagentless production of a promising material with outstanding physicochemical features to create novel electrochemical sensors and biosensors. This review addresses different strategies for fabricating laser-scribed graphene (LSG) devices and their association with nanomaterials, polymers, and biological molecules. We provide an overview of their applications in environmental and health monitoring, food safety, and clinical diagnosis. The advantages of their integration with machine learning models to achieve low bias and enhance accuracy for data analysis is also addressed. Finally, in this review our insights into current challenges and perspectives for LSG electrochemical sensors are presented.

Keywords: laser scribing graphene; electrochemical sensors; chemical sensing; biochemical sensing

Citation: Ameku, W.A.; Negahdary, M.; Lima, I.S.; Santos, B.G.; Oliveira, T.G.; Paixão, T.R.L.C.; Angnes, L. Laser-Scribed Graphene-Based Electrochemical Sensors: A Review. *Chemosensors* **2022**, *10*, 505. https://doi.org/10.3390/chemosensors10120505

Academic Editor: Dan Xie

Received: 29 October 2022
Accepted: 24 November 2022
Published: 29 November 2022

1. Introduction

The laser scribing technique induces high-carbon precursors into highly conductive porous graphene-like sheets structured three-dimensionally by direct, single-step, and mask-free laser writing without needing a controlled environment [1,2]. The process is fast and convenient to pattern carbon tracks, allowing upscaling for mass production and device miniaturization without requiring reagents, which sets very favorable conditions for developing green processes [3].

Various materials are used as substrates for carbon sources; usually a polymer, which can be synthetic or natural. Possible substrates include the following: polyimide (PI), polyetherimide (PEI), polysulfone, paperboard, phenolic paper, potato skin wood, face masks, cork, coconut, nail polish, carboxymethylcellulose, aramid fabric, and cloth [4–8]. In the process of fabrication, a CO_2 laser (wavelength about ~10.6 µm) is primarily employed, but, likewise, ultraviolet (UV) and visible lasers can be used to prepare the 3D graphene sheets [9].

Laser-scribed graphene (LSG) is named by several terms, including laser-induced graphene, laser-ablated graphene, laser-derived graphene, laser-burned graphene, laser-engraved graphene, or laser-enabled graphene [1,2,10,11]. It has increased edge plane/defect sites that are very beneficial for heterogeneous electron transfer, yielding increased current densities and reduced overpotentials for some electroactive species, which include inner (i.e., ferricyanide) and outer (i.e., 1,1′-ferrocene dimethanol) sphere redox probes [12]. Its electrochemical activity is compared to edge plane pyrolytic graphite (i.e., a carbon-based material that shows conspicuous electroactivity and often presents advantages over carbon nanotubes) [12]. LSG conserves the reversible nature of ferricyanide, resulting in a peak-to-peak difference (ΔE_p) of 56.3 mV, high heterogeneous electron transfer rate constant (k_0) of 3.2×10^{-2} cm s^{-1}, and 3.4-fold more significant electroactive area than electrode geometric area [13].

The laser scribing method circumvents ink formulation, as required for screen-printed electrode fabrication, and it circumvents the annealing steps, commonly associated with graphene-based devices, and the need for multiple pieces of laboratory equipment and chemicals associated with the complex and more protracted fabrication process for chemical graphene synthesis [14]. Furthermore, it eliminates the necessity for a high-temperature, low-pressure atmosphere, and metal seed catalysts, usually related to graphene-based device fabrication through chemical vapor deposition processes [15].

LSG affords high charge mobility and specific surface area, appealing features to apply in multiple fields. In the energy storage field, it yields higher power densities and mechanical rigidity, improving lithium-ion batteries as the porous carbon anodes, where the lithium ions are inserted to store energy, are very effective [11]. Supercapacitors were made from LSG-graphitic electrodes, showing superior energy and power performance to that of conventional supercapacitors [16]. LSG was applied to make up glucose biofuel cells, and the electrode was integrated with active catalytic nanomaterials to take advantage of the biochemical energy of glucose [17]. Applying a non-thermal laser scribe method on graphene oxide (GO)/silver nanowires (SNWs) thin film reduced it to rGO/SNW, resulting in 80% transparency and 70 Ω cm^{-1} sheet resistance that could be used as an optoelectronic device [18]. When Cu_xO nanoparticle were immobilized on LSG a highly efficient and inexpensive electrocatalyst for hydrogen production resulted [19]. In the biomedical field, concerning airborne hazard microorganisms, LSG can be engraved on commercial surgical masks to inactivate pathogens by increasing surface temperature due to graphene's excellent photothermal activity in the near-infrared region. LSG can also confer superhydrophobic and self-cleaning capability to fabricated multi-usage masks [4].

Likewise, the laser-scribing process produces friendly to use and disposable devices for sensor applications. Disposable devices ultimately end up in landfills or, in the worst case, in forests or oceans; thus, developing them with recyclable, biodegradable, environmentally friendly materials, preferably consisting of CO_2-cycle origin carbons is highly advantageous [16]. The paperboard surface was directly pyrolyzed, producing conductive porous non-graphitizing carbon material comprised of graphene sheets decorated with aluminosilicate nanoparticles in-situ synthesized and originated from the kaolin precursor, a product commonly used as a paper additive, coating, and pigment in the industry (Figure 1A) [3]. The paperboard sensor exhibited superior electrochemical performance to that of glassy carbon and carbon screen-printed electrodes (SPEs). Moreover, it was applied as a proof-of-concept to detect relevant compounds for the food and dietary supplements industries and homeland security (i.e., ascorbic acid (AA), caffeic acid, and picric acid). Nevertheless, paper usage for fabricating LSG is not so common because it remains challenging, due to the paper's composition, cellulosic structure, and grammage [3].

In other research, a green and sustainable SPE, made using cellulose/lignin-based ink patterned on a polyethylene terephthalate substrate, was graphitized by the CO_2 laser (at ambient conditions), enabling it to reach the low sheet resistance to be applied as a humidity sensor [16]. Interestingly, instead of using the laser treatment to graphitize, it was used to remove debris and original binder materials, thereby improving the graphite layer's defects, when transferred to an office paper surface by the pencil drawing technique (Figure 1B). This enhanced the electrochemical performance by increasing the electroactive area and facilitating heterogeneous electron transfer, which allowed the detection of diuretic medicine furosemide in synthetic urine [17].

By coupling LSG electrochemical sensors to machine learning (ML) models, it is possible to achieve rapid data acquisition, and the intelligent and automated analysis of large amounts of data, with accurate results [18,19]. The association of mathematical and statistical methods to analyze, process, and extract crucial information from large complex datasets can be fundamental in complex cases [20]. These algorithms provide techniques to automatically identify patterns in a dataset, allowing models to predict, based on them, with low bias, and reducing the error. The prowess of ML algorithms lies in their capacity to learn and automate the extraction of information from a given dataset, which usually

requires a domain specialist to be identified [20]. The flexibility and toughness of these algorithms allow them to adapt to any application that has the basic requirement of an arbitrary dataset. ML algorithms can be excellent candidates to replace traditional detection approaches with expanding datasets [20].

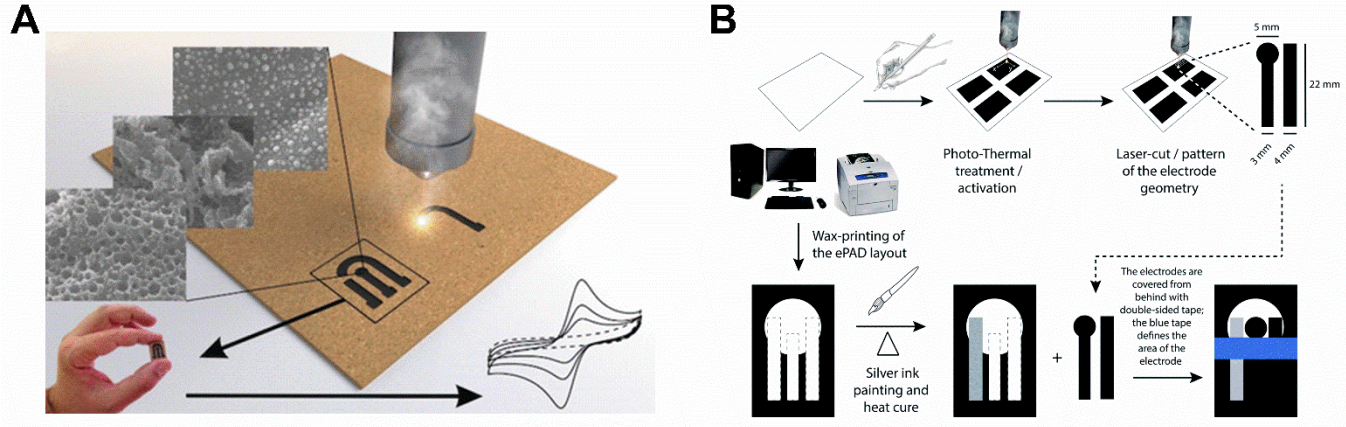

Figure 1. (**A**) Schematic representation of the laser manufacturing process of LSG-based electrodes made on paperboard [3]. License number: 5432010483088 (**B**) Graphic representation of the manufacturing steps and laser treatment of electrodes prepared by the pencil drawing technique. Adapted with permission from [17].

Various review articles have provided comprehensive descriptions of, and demonstrated, LSG technology's versatility in numerous applications. Thamaraiselvan et al. focused on applying LSG and carbon nanotubes in water treatment [21]. Lahcen et al. showed recent advancements in applying LSG to electrochemical sensing and biosensing [10]. Han et al. presented an interesting revision addressing the applications of LSG to build a flexible platform for sensing [22]. Several other illuminating review articles highlighted contributions to LSG technology [23–27]. In the same way, in the smart sensing field, numerous review articles have brought up recent advances [28–30]. Ha et al. reviewed the ascent of smart sensing systems and their future challenges and opportunities [20]. Cui et al. reviewed the main advances in biosensors combined with ML [31]. In this review, we emphasize the advances occurring from 2017 to mid-2022 for chemical and biochemical sensing using the emerging technology of LSG to build electrodes and, also, their use, combined with ML, in relevant fields, such as environmental and health monitoring, clinical diagnosis, and food safety.

2. Graphene Preparation Methods

The usual methods for altering graphene characteristics include chemical vapor deposition (CVD) and the wet-chemistry process. CVD is performed at high temperatures, limiting the types of substrates used for growing graphene [11]. Therefore, additional steps are required to transfer graphene onto other substrates which are not very resistant to high temperatures (e.g., paper or plastics). The wet-chemistry process includes a synthesis route to produce graphene/graphene oxide through methods that frequently comprise pyrolysis or acid etching, as used in the Hummer's or Brodie methods [14]. Both processes require high temperatures.

Laser irradiation in the LS photothermal process produces a localized high temperature (up to 2000–2500 °C) [3,32]. The high temperatures result in lattice vibrations of the substrate surface elements. This thermal treatment fragments the C–O, C=O, and N–C bonds of the PI surface substrate during the process. These atoms are liberated as gases and, in sequence, are recombined to form graphitic structures [32]. In most cases, airflow during the process is used to keep the substrate surface clean, avoid dirtying the laser machine lens, and remove the possible evolved gasses.

The resulting material presents structured characteristics with a rough graphene surface having a surface area of ~340 m^2 g^{-1}, high thermal stability (>900 °C), and excellent electrical conductivity (5~25 S cm^{-1}), which is analogous to 3D graphene produced via wet-chemistry [11]. LSG has an unusual polycrystalline structure, which occurs in a mixture of the hexagon and pentagon–heptagon hybrid lattice instead of the classical hexagon lattice only. It happens probably because of the rapid chilling after laser irradiation without time for equilibration to form the standard hexagon lattice; this process was denominated kinetic graphene [25].

The final attributes of materials strongly depend on the precursors' physical and chemical structures [32]. Pyrolyzing organic molecules with oxygen-high content (e.g., cellulose and sucrose) in environmental conditions generates non-graphitizing carbons, for instance [3]. However, the morphology of a given material can be easily adjusted by manipulating software to obtain desired properties, and parameters, such as the laser's scan rate, power, and output distance, can be changed [11].

The lasing parameters influence the controlling of LSG's chemical and physical features. At an energy density of 4.1 J cm^{-2} equals 8 W and 33.2 J cm^{-2}, 64 W [33] LSG starts to form on the PI [25]. Generally, the higher the laser power, the thicker and more conductive the LSG layer is; however, the substrate can be completely burned if the power is excessively high [25]. Some studies indicate that by increasing the laser power, the laser scanning speed must also be enhanced to achieve graphitization, while avoiding the total burning of PI. [33] Interestingly, it was noticed that when the applied laser power was increased, the porosity of the N-doped LSG improved (Figure 2A) [34]. Other factors influencing LSG morphology are the pulses per inch (PPI), and the lines per inch (LPI). According to Ye et al. [29], when the relation of 1000 PPI × 1000 LPI and a ~100 µm laser spot size is used, the LSG adopts an in-plane porous structure. At 500 PPI × 500 LPI with a ~60 µm laser spot size, the LSG starts to produce out-of-plane fibers and forms a vertically aligned forest morphology.

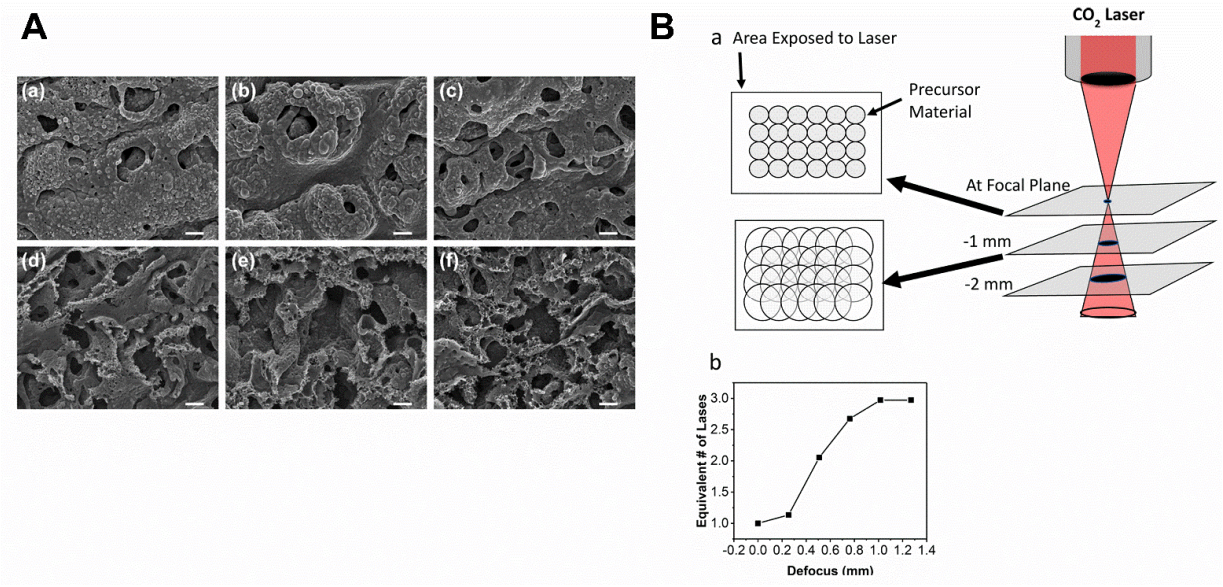

Figure 2. (**A**) Scanning electron micrograph images of the N doped-LSG electrodes after laser scribing process using laser power of (**a**) 2.8%, (**b**) 3.2%, (**c**) 3.6%, (**d**) 4.0%, (**e**) 4.4%, (**f**) 4.8%, all the scale bars are four µm. Reprinted with permission from [34]. Copyright 2020 American Chemical Society (**B**) (**a**) The diagram shows defocus effect by increasing laser spot size. No dot overlapping was seen at low DPI (less than 150) and in the focal condition. Increasing the defocus caused more overlap due to larger point sizes, causing numerous exposures. The defocus condition can also be achieved by moving the substrate above or under the focal plane. (**b**) The equivalent number of laser exposures at various defocus ranges. Reprinted with permission from [8]. Copyright 2018 American Chemical Society.

The usage of the defocused laser scribing method can influence the LPI parameter; rendering a more uniform energy distribution, which is beneficial (Figure 2B). It increases the laser's spot size and keeps the density of the dots consistent. Thus, it results in multiple lines in a single laser's pass in each location of the substrate, further simplifying the procedure and increasing processing pace, since each spot can be placed many additional times in one laser pass [8,35].

3. Fabrication of the LSG Electrodes

3.1. LSG from Polymer Treatment

Based on the data compiled in Table 1, LSG is commonly produced using a synthetic polymer substrate, the most used one is PI, and the CO_2 laser (10.6 μm) is frequently used. The applied laser power ranges from 1.65 W to 40 W, and the scan rate range is 3.5 mm s^{-1}–108 cm s^{-1}. When a laser with high power is used, a high scan rate is often required to avoid the complete burning of the substrate and, thus, obtain adequate pyrolysis. The laser output height (z-distance) ranges from 0.1–74 mm, which modulates the laser beam size; thus, the laser can be used focused or unfocused. The process is carried out in most cases under ambient conditions, rarely under inert gas; this condition could be used to decrease the heteroatom bonding effect (Figure 3A) [36]. Other substrates, such as carbon black/polylactic acid, phenolic paper, and lignin/poly(vinyl alcohol) are also used, as well as lasers with different wavelengths e.g., 355, 405, and 450 nm. The application in chemical and biochemical sensing is quite diverse. Some experimental conditions are compiled in Table 1.

3.2. LSG from 3D-Printed Electrode

About 90% of 3D-printed electrodes' conductive filaments composition is a non-conductive thermoplastic material; thus, they provide slow electrochemical transfer [37]. To improve performance, removing non-conductive materials and exposing electroactive sites is obligatory. One of the removal ways is with organic solvent followed by electrochemical treatment; however, the compounds used are not eco-friendly, and it is a time-consuming process [37]. Therefore, the laser treatment of 3D electrodes, was reported for the first time. The carbon black/PLA-based 3D printed device was, without reagents, treated with a CO_2 laser (10.6 μm) to eliminate the non-conductive fraction. The treatment used a laser power of 350 mW, a scan rate of 20 mm s^{-1}, a height of 10 mm, and lasted about 50 s [37].

3.3. LSG from Phenolic Resin

Phenolic resin can be utilized as a substrate for direct laser scribing using different wavelengths. The resultant material possesses attractive properties, such as low resistance, porosity, and good mechanical properties. It was applied in diverse fields, including sensing, energy storage, electrothermal conversion, and electronic device development [38–41]. Therefore, a CO_2-laser cutter system with a pulse duration of ∼14 μs in an optimized condition (laser power: 2.1 W; scan rate: 8.5 mm s^{-1}; and Z-distance: 12.0 mm) was used for engraving LSG on phenolic paper [38]. After the engraving process, the electrode was subjected to electrochemical treatment, applying a potential of −1.0 V for 60 s in 1.0 mol L^{-1} KCl solution, to improve the electrochemical properties. Another work used a 405 nm laser to engrave conductive trails on substrates, such as polyethylene terephthalate, glass slides, and sticky notes coated with phenolic resin previously dispersed in ethanol [39]. The optimized condition was laser height: 90 mm; laser power: 500 mW; scan rate: 200 mm/s. Another study used flexible phenolic and phenolic blended with polyvinyl alcohol films, which demonstrated promising applicability as a touch and pressure sensor [40]. Lasered-carbon tracks on phenolic resin with Prussian blue film demonstrated great electrothermal properties yielding a notorious Joule heating effect at a low applied potential [41].

Table 1. Collection of different approaches to laser scribing methods for manufacturing LSG electrodes.

Electrode	Substrate Material	Laser Source	Laser Wavelength	Laser Power	Scan Rate	z-Distance	Ambient Condition	Electrochemical Application	Reference
NP-LIG or Cu^{2+}/NP-LIG	NP	NA	405 nm	3 W	NA	60 mm	air	Chemical sensing	[5]
LSG	PEI	CO_2	NA	10.5%	40 mm s^{-1}	10 mm	NA	Chemical sensing	[13]
LIG	PI	CO_2	NA	5.25 W	271.9 mm s^{-1}	2 mm	NA	Chemical sensing	[14]
LIG	PI	CO_2	NA	4%	7%	74 mm	air	Biochemical sensing	[15]
ePAD	GRA	CO_2	10.6 µm	500 mW	25 mm s^{-1}	10 mm	air	Chemical sensing	[17]
ACE2-AuNP/LSG	PI	CO_2	10.6 µm	3.2 W	2.8 cm s^{-1}	2.5 mm	N_2 gas	Biochemical sensing	[19]
LSG/MIP	PI	CO_2	10.6 µm	3.2 W	2.8 cm s^{-1}	2.5 mm	air	Chemical sensing	[32]
N-LIG	PI	CO_2	10.6 µm	32 W	108 cm s^{-1}	NA	air	Biochemical sensing	[33]
Enzyme/Ti_3C_2Tx/PB/N-LSG	Lign/PVA/UR	CO_2	10.6 µm	4.8%	3%	2.4 mm	air	Biochemical sensing	[34]
LIG@Ag	PI	NA	NA	4.2 W	50 mm s^{-1}	10 mm	NA	Chemical sensing	[35]
LSG	PI	CO_2	10.6 µm	3.2 W	2.8 cm s^{-1}	2.5 mm	Inert gas	Biochemical sensing	[36]
3D-printed CB/PLA	CB/PLA	CO_2	10.6 µm	350 mW	20 mm s^{-1}	10 mm	NA	Chemical sensing	[37]
LS-ET-PR	PR	CO_2	10.6 µm	2.1 W	8.5 mm s^{-1}	12.0 mm	air	Chemical sensing	[38]
PCE	PR	CO_2	10.6 µm	12 W	300 mm s^{-1}	NA	NA	Chemical sensing	[41]
PFA/GO	PFA/GO	CO_2	NA	3.88 W	100 mm s^{-1}	NA	NA	Chemical sensing	[42]
N, O doped LIG	PI	NA	355 nm	2.5 W	30 mm s^{-1}	NA	air	Chemical sensing	[43]
LSG/f-MWCNT-AuNPs	PI	NA	405 nm	2W	50 mm s^{-1}	NA	air	Chemical sensing	[44]
LSG	PI	CO_2	10.6 µm	1.65 W	3.5 mm s^{-1}	NA	air	Chemical sensing	[45]
Fe_3O_4/$MWCNT_S$/LSG/CS/GCE	PI	NA	NA	40 W	100 mm s^{-1}	0.1 mm	air	Chemical sensing	[46]
LSG	PI	NA	450 nm	5.23 W	5.5 mm s^{-1}	NA	air	Chemical sensing	[47]
h-BN/$LIPG_0$	PI	NA	450 nm	NA	NA	NA	air	Chemical sensing	[48]
LEGCN	PI	CO_2	NA	6.4 W	50 mm s^{-1}	NA	NA	Chemical sensing	[49]
ZVO/SGN-LGE	PI	CO_2	10.6 µm	3.2 W	2.8 cm s^{-1}	2.5 mm	NA	Chemical sensing	[50]
AuNPs-LIG	PI	NA	NA	2.20–3.85 W	1–3 cm s^{-1}	NA	air	Biochemical sensing	[51]
MoS_2/S-Ti_3C_2/LGE	PI	CO_2	10.6 µm	3.2 W	2.8 cm s^{-1}	2.5 mm	NA	Biochemical sensing	[52]

Table 1. *Cont.*

Electrode	Substrate Material	Laser Source	Laser Wavelength	Laser Power	Scan Rate	z-Distance	Ambient Condition	Electrochemical Application	Reference
LI-CdS-G@GC	GCE	CO_2	10.6 µm	6.0 W	166 mm s^{-1}	NA	air	Chemical sensing	[53]
N@LEG/GCE	PI	CO_2	NA	5 W	50 mm s^{-1}	NA	air	Chemical sensing	[54]
Pt/LSG	PI	CO_2	10.6 µm	15%	10%	2 mm	air	Chemical sensing	[55]
PEDOT-LSG	PI	CO_2	10.6 µm	4.6 W	0.56 cm s^{-1}	2 mm	air	Chemical sensing	[56]
LIPG	PI	NA	NA	5.2 W	0.4 cm s^{-1}	NA	NA	Chemical sensing	[57]
Ti_3C_2Tx-LIG-IDE	PI	NA	NA	3.85 W	2 cm s^{-1}	NA	NA	Chemical sensing	[58]
Ti_3C_2-MXene/BP/LIPG	PI	NA	NA	5.2W	NA	10 mm	air	Chemical sensing	[59]
LIPG	PI	NA	NA	5.5 W	0.5 cm s^{-1}	NA	NA	Chemical sensing	[60]
PI-LIG	PI	NA	10.6 µm	50%	50%	NA	NA	Chemical sensing	[61]
SnO_2/CeO_2/LIG	PI	NA	NA	NA	NA	NA	NA	Chemical sensing	[62]
LIG–CS–AuNPs	PI	CO_2	10.6 µm	1.8 W	160 mm s^{-1}	6 mm	air	Chemical sensing	[63]
eMoS$_x$-LIG	PI	CO_2	NA	10.5%	5.5%	NA	NA	Biochemical sensing	[64]
Nafion/Fe_3O_4/LSG	PI	NA	10.6 µm	5.4 W	NA	5 mm	NA	Chemical sensing	[65]
LSG	PI	NA	10.6 µm	0.81 W	5.8 cm·s^{-1}	2 mm	air	Biochemical sensing	[66]
AuNPs-LIG	PI	CO_2	NA	8%	NA	NA	NA	Biochemical sensing	[67]
Co_3O_4 NPs-LIG	PI	CO_2	NA	NA	NA	NA	NA	Chemical sensing	[68]
Chit-Au-LIG	PI	CO_2	NA	5%	NA	6 mm	air	Biochemical sensing	[69]
DLEG	PI	CO_2	NA	3.9 W	NA	5 mm	air	Chemical sensing	[70]
PtNPs/PAAMI/LAG	PI	CO_2	NA	17 W	60 mm s^{-1}	NA	air	Biochemical sensing	[71]
Pt-LIG	PI	CO_2	NA	7%	7%	2 mm	NA	Biochemical sensing	[72]
LIG	PI	CO_2	NA	60%	15%	NA	NA	Biochemical sensing	[73]
µPAD	CP	CO_2	10.6 µm	6.5%	12 mm s^{-1}	12 mm	air	Chemical sensing	[74]
Pt-AuNPs/LIG/PDMS	PI/PDMS	CO_2	NA	7.6 W	200 mm/s	NA	NA	Chemical sensing	[75]

Abbreviations—ACE2: angiotensin converting enzyme 2; AuNP: gold nanoparticle; BP: phosphorene; CB/PLA: blend of carbon black and polylactic acid; CS: Chitosan; CP: Chromatographic paper; eMoSx: electrodeposited molybdenum polysulfide; ET: electrochemical treatment; G: graphene; GC: glassy carbon electrode; GO: graphene oxide; GRA: graphite; h-BN: Hexagonal boron nitride 2D material; f-MWCNT: COOH functionalized multiwalled carbon nanotube; LEG: laser engraved graphene; LEGCN: laser etched to obtain graphene-based carbon nanomaterial; LGE: laser-induced graphene electrode; LI: laser-induced; LIG: Laser-induced graphene; Lign: lignin; LIG-IDE: laser-induced graphene interdigital electrode; LIPG: laser-induced porous graphene; LS: Laser scribed; LSG: Laser-scribed graphene; MIP: Molecularly imprinted polymers; NA: not available; N-LSG: nitrogen-doped laser-scribed graphene; NP: nail polish; PCE: porous carbon electrode; PEDOT: poly(3,4-ethylenedioxythiophene); PEI: polyetherimide; PES: Poly(ether-Sulfone); PFA: poly(furfuryl alcohol); PI: polyimide; PR: phenolic resin; PVA: poly(vinyl alcohol); SGN: sulfur doped carbon nitride; S-Ti3C2: sulfur-doped Ti3C2 MXene nanocatalyst; Ti3C2-MXene: graphene-like titanium carbide MXene; UR: urea; ZVO: 3D zinc vanadate.

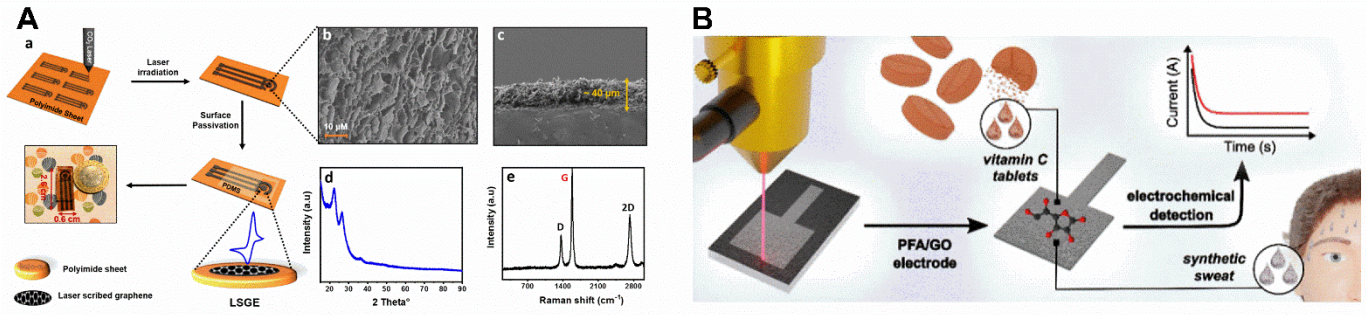

Figure 3. (**A**) (**a**) Graphic description of the manufacture of LSG based on laser scribing of the PI substrate under inert gas condition; (**b**,**c**) Scanning electron micrograph image of the resulted LSG and cross-section of LSG electrode; (**d**) X-ray diffraction spectrum of LSG device; (**e**) Raman Spectrum of LSG electrode [36]. License number: 5432021450144 (**B**) Direct laser engraving of graphene oxide-biomass-derived poly(furfuryl alcohol) electrode for non-enzymatic electrochemical detection of ascorbic acid in vitamin C pills and synthetic sweat [42]. License number: 543203029591.

3.4. LSG from Graphene Ink

LSG can be obtained from the laser treatment of graphene or its analogous ink. Thus, a graphene ink, formulated by mixing graphene and reduced graphene oxide (GO) powders in cyclohexane and terpineol with posterior addition of ethyl cellulose, was inkjet printed on PI or photo paper [41]. The graphene layer printed film was treated with a pulsed laser (15 ns) of 355 nm wavelength to anneal and nanostructure the electrode. Alternatively, GO prepared by Hummer's method was mixed with furfuryl alcohol (PFA), and the resulting poly condensed PFA/GO was used to coat a glass substrate, followed by CO_2 laser treatment to carbonize the electrode pattern using 3.88 W of laser power and 100 mm s^{-1} scan rate (Figure 3B) [42].

3.5. Element Doped LSG

A practical method to co-dope LSG with N and O was reported. It was performed using an ultraviolet irradiation laser of 355 nm wavelength on PI in the air without any modifications at laser focus. The laser frequency, power, scan rate, and gap line were 70 kHz, 2.5 W, 30 mm s^{-1}, and 40 µm, respectively [43]. Another method performed under the air was also reported. A CO_2 laser cutting machine with a beam size of the laser at roughly 70 µm was employed to treat the PI sheet under ambient conditions. High laser power (32 W) and scan rate (108 cm s^{-1}) with 1000 pulses per inch (PPI; 1000) were used to dope LSG [33]. Another way to produce N-doped LSG treated a plastic support (e.g., polycarbonate and poly (ethylene terephthalate)) coated with a film comprising lignosulfonate, PVA, and urea, with a CO_2 laser cutting machine [46].

4. Approaches to Modify LSG Electrochemical Sensors

4.1. LSG Modified by Nanostructured Materials and Polymers and Its Use as a Modifier of Conventional Electrodes

One-step silver nanoparticle-modified LSG was reported. A defocused laser scribing method was used. Previously, the PI film was treated with an ultraviolet laser to create roughness and, thus, increase its wettability. Then, $AgNO_3$ solution was drop-cast on the PI film and dried in the air. The dried film was then treated by laser process, with a power of 4.2 W, step size of 1064 nm, and scan rate of 50 mm s^{-1}, to produce LSG modified with Ag [35]. In a similar approach, a hydrogel ink, made of chitosan and a solution of $HAuCl_4$, $AgNO_3$, or H_2PtCl_6, was utilized to coat PI film, and, after drying, a laser was scribed to modify LSG with nanoparticles (Figure 4A) [51].

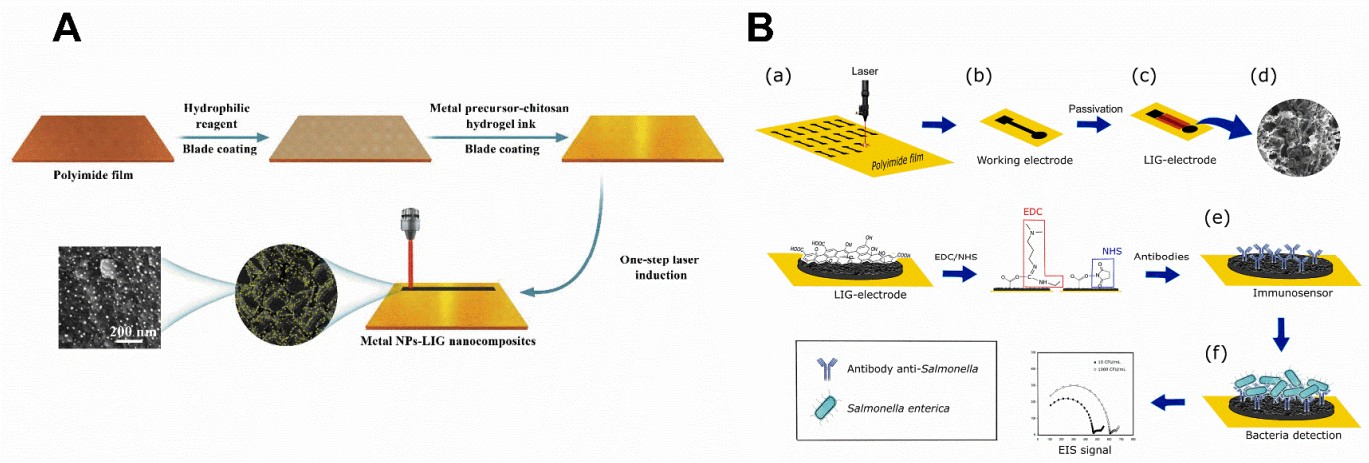

Figure 4. (**A**) Graphic representation of the nanoparticle-LSG hybrid nanocomposites fabrication using the single-step laser engraving procedure [51]. License number: 5432030508595 (**B**) Representative scheme of LSG immunosensor for *S. enterica* detection. (**a**,**b**) Manufacture of working electrode, (**c**) passivation of the electrode with lacquer, (**d**) scan electron micrograph image showing the LSG surface, (**e**) modification with *S. enterica* antibodies attached on the working electrode via EDC/NHS coupling, and (**f**) *S. enterica* binding to the electrode, and the resultant impedance signal generated during assay. Reprinted with permission from [15]. Copyright 2020 American Chemical Society.

Molecularly imprinted polymers (MIPs) have cavities with high selectivity to a molecule of interest, such as natural biological receptors, antibodies, and enzymes, which can be combined with LSG to couple the rapid production of multilayer graphene and provide excellent conductivity [32]. The MIP can be electropolymerized using 2 mM pyrrole in phosphate buffer saline (PBS) with the target molecule as the template; some research used 0.01 mM of bisphenol A as template [32].

The produced LSG can be used as modifier of conventional electrodes. Thus, PI sheets can be laser etched to produce graphene-based nanomaterials. The obtained LSG was used to coat conventional glassy carbon electrodes (GCEs) to improve electrochemical performance. An LSG-modified GCE with bismuth film demonstrated superior performance in detecting heavy metals, such as Cd^{2+} and Pb^{2+} [49]. By mixing LSG with Fe_3O_4, multi-walled carbon nanotubes (MWCNTs), chitosan (CS), and in-situ plating bismuth film (BF), a novel nanocomposite with remarkable electrochemical performance to coat GCE was obtained for the simultaneous and selective detection at trace level of Cd^{2+} and Pb^{2+} in tap water using square wave anodic stripping voltammetry (SWASV) [46].

4.2. LSG Electrodes Modified with Biological Molecules

Most approaches to functionalizing LSG electrodes with biological molecules use a linker molecule and then carry out the EDC/NHS chemistry. For that, a gold-modified LSG can be carbonylated using 11-mercaptoundecanoic acid to allow anchoring of carcinoembryonic antibodies [76]. Cysteamine molecules can be used as a linker to allow severe acute respiratory syndrome virus 2 (SARS-CoV-2) antibodies' [77] and angiotensin converting enzyme 2 (ACE2) [19], immobilization to Au-modified LSG. Another alternative is using a 1-pyrenebutyric acid (PBA) linker. The PBA anchored directly to the LSG functionalized the surface of the LSG with carbonyls, which allowed anchoring of the antibodies of SARS-CoV-2 nucleocapsid protein, C-reactive protein and capture spike proteins of immunoglobulin to develop the COVID-19 electrochemical sensor [78]. Using PBA, an amino-functionalized aptamer can also be immobilized as a biorecognition element [66].

A cationic polymer, such as polyallylamine rich in amine groups, can also be used to coat the LSG for antibody immobilization. They were anchored through EDC/NHS to allow biomarker detection (Figure 4B) [71]. A direct immobilization of anti-*Salmonella* on LSG through EDC/NHS was also reported. [15] On the other hand, direct immobilization

of antibodies on the Au-modified LSG without using EDC/NHS was reported where a drop of a solution of goat anti-*E. coli* O157:H7 antibody was added to the electrode and incubated overnight at 4 °C [51].

5. Analytical Methods

5.1. Electrochemical Tools

Table 2 shows the analytes detected using the LSG-based material and the respective electroanalytical techniques, dynamic ranges, and limit of detection (LOD). The applications range from small analytes, such as hydrogen, sodium, potassium, and heavy metals ions [37,73], to microorganisms, such as *E. coli* bacteria [51], and macromolecules such as antibodies [71]. The most frequently used techniques are differential pulse voltammetry (DPV), square wave voltammetry (SWV), and amperometry (AMP). For example, DPV was used to detect antibodies by suppressing the signal of the mediator molecule $Fe(CN)_6^{3-/4-}$, [71] SWV was used to detect heavy metals by anodic stripping [37], and amperometry to detect H_2O_2 [35].

Table 2. Compilation of analytical characteristics of LSG electrochemical sensors.

Electrode	Analyte	Technique	LOD	Dynamic Range	Machine Learning Model	Reference
NP-LIG or Cu^{2+}/NP-LIG	Nit and GLU	Nit: DPV GLU: AMP	0.9 µM	2.0–1000 µM	NA	[5]
PEI-LSG	HQ, PA, MP	SWV	HQ: 9.42×10^{-8} mol L^{-1} PA: 3.23×10^{-7} mol L^{-1} MP: 2.95×10^{-7} mol L^{-1}	HQ, PA, MP: 10–50 µ mol L^{-1}	NA	[13]
LIG	CLO, IMD, TMX, DNT	SWV	CLO: 823 nM IMD: 384 nM TMX: 338 nM DNT: 682 nM	10−40 µM	NA	[14]
LIG	*S. enterica*	EIS	13 ± 7 CFU mL^{-1}	25–10^5 CFU mL^{-1}	NA	[15]
ePADs	FUR	DPV	2.4×10^{-7} M	25–196 mM	NA	[17]
ACE2-AuNP/LSG	S1 and S2	DPV	S1: 5.14 ng/mL S2: 2.09 ng/mL	1.0–200 ng/mL	DNN	[19]
MIP/PPy@LSG	BPA	DPV	8 nM	0.5–5 mM	NA	[32]
N- LIG	miRNA	DPV	10 fM	10 fM–10 nM	NA	[33]
Enzyme/Ti_3C_2Tx/PB/N-LSG	LAC ALC GLU	AMP	LAC:0.5 µM ALC: NA GLU: 0.3 µM	0–20 mM 0–50 mM 10 µM–5.3 mM	NA	[34]
AgNPs-LIG	H_2O_2	AMP	2.8 µM	0.01–2.61 mM	NA	[35]
LSG	PAR	SWV	31 nM	0.1 µM–10 µM	NA	[36]
3D-printed CB/PLA	Cd^{2+}, Pb^{2+}, Cu^{2+}	SWASV	$Cd^{2+:}$ 1.34 µg L^{-1}, Pb^{2+}: 1.32 µg L^{-1}, Cu^{2+}: 0.31 µg L^{-1}	Cd^{2+}, Pb^{2+}, Cu^{2+}: 25–125 µg L^{-1}	NA	[37]
LSG	β-ED	DPV	12.1 mM	0.1–1 mM	NA	[38]
PCE	Nit DA	CV	Nit: 0.173 mM DA: 0.136 mM	Nit: 0.2–1 mM DA: 0.2–1 mM	NA	[41]
PFA/GO	AA	AMP	1.0 µmol cm^2 L^{-1}	50–5000 µmol L^{-1}	NA	[42]
N, O doped LIG	Nit	DPV	0.8 µmol/L	5–450 µmol/L	NA	[43]
LIG/f-MWCNT-AuNPs	NO_2^-	SWV	0.9 µM	10–140 µM	NA	[44]
LSG	HYD	CV	70 µM	0.1–0.5 mM	NA	[45]
Fe_3O_4/$MWCNT_S$/LSG/CS/GCE	Cd^{2+} Pb^{2+}	SWASV	Cd^{2+}: 0.1 µg L^{-1} Pb^{2+}: 0.07 µg L^{-1}	1–200 µg L^{-1}	NA	[46]
LSG	XT HX	DPV	XT: 0.26 µMHX: 0.18 µM	XT: 0.3–179.9 µM HX: 0.3–159.9 µM	ANN	[47]
h-BN/$LIPG_0$	SMZ	DPV	0.011 µM	0.5–362.5 µM	NA	[48]

Table 2. *Cont.*

Electrode	Analyte	Technique	LOD	Dynamic Range	Machine Learning Model	Reference
LEGCN	Cd^{2+} Pb^{2+}	SWASV	Cd^{2+}: 0.47 µg L^{-1} Pb^{2+}: 0.41 µg L^{-1}	Cd^{2+}: 7–120 µg L^{-1} Pb^{2+}: 5–120 µg L^{-1}	NA	[49]
ZVO/SGN-LGE	NFT CAP	DPV	NFT: 2.4 nM CAP: 1.5 nM	NFT: 0.005–325.5 µM CAP: 0.005–187.5 µM	NA	[50]
AuNPs-LIG	*E. coli* 0157:H7	EIS	1×10^2 CFU mL^{-1}	1×10^2– 1×10^8 CFU mL^{-1}	NA	[51]
MoS_2/S-Ti_3C_2/LGE	ARA ROX	DPV	ARA: 1.65 nM ROX: 2.31 nM	0.01−875.01 µM	NA	[52]
LI-CdS-G@GC	I^-	ECL	4.0 nM	10.0–2500 nM	NA	[53]
N@LEG/GCE	Cd^{2+} Pb^{2+}	SWASV	Cd^{2+}: 1.08 µgL^{-1} Pb^{2+}: 0.16 µgL^{-1}	Cd^{2+}: 5–10 µg L^{-1} and 10–380 µg L^{-1} Pb^{2+}: 0.5–10 µgL^{-1} and 10–380 µgL^{-1}	NA	[54]
Pt/LSG	AA DA UA	DPV	AA: 6.1×10^{-6} M DA: 0.07×10^{-6} M UA: 0.22×10^{-6} M	AA: 10–890 $\times 10^{-6}$ M DA: 0.5–56 $\times 10^{-6}$ M UA: 1–63 $\times 10^{-6}$ M	NA	[55]
PEDOT-LSG	DA	DPV	0.33 µM	1–150 µM	NA	[56]
LIPG	MH	DPV	NA	NA	LSSVM	[57]
Ti_3C_2Tx-LIG-IDE	MeOH, EtOH, IPA, ACET	EIS	NA	100–800 ppm	PCA, LDA and PLS	[58]
Ti_3C_2-MXene/BP/LIPG	NAA	LSV	1.6 nM	0.02–40 µM	ANN	[59]
LIPG	SA	LSV	0.16 µM	0.5 µM–500 µM	LSSVM	[60]
PI-LIG	Pb(II)	ASV	50 ppb	NA	NA	[61]
SnO_2/CeO_2/LIG	Cd(II)	DPASV	0.01 µg/L	0.1–160 µg/L	NA	[62]
LIG–CS–AuNPs	UA	DPAdSV	0.33 µmol L^{-1}	1.0–30 µmol L^{-1} and 30–100 µmol L^{-1}	NA	[63]
eMoS_x-LIG	UA and TYR	DPV	TYR: 100 nM UA: 10 nM	NA	DT	[64]
Nafion/Fe_3O_4/LSG	CQL	DPV	0.73 nmol L^{-1}	1 nmol L^{-1}– 100 mol L^{-1}	NA	[65]
LSG	TRB	DPV	1 pmol L^{-1}	1–100 pmol L^{-1}	NA	[66]
AuNPs-LIG	PRX	DPV	1.2 ng mL^{-1}	3–4000 ng mL^{-1}	NA	[67]
Co_3O_4 NPs-LIG	GLU	AMP	0.41 µM	1 µM–9 mM	NA	[68]
Chit-Au-LIG	UA	DPV UA	0.5 M	NA	NA	[69]
DLEG	AA	CV	3.8 mol L^{-1}	30–1100 mol L^{-1}	NA	[70]
PtNPs/PAAMI/LAG	IgG	DPV	6 pg mL^{-1}	0.012–352 ng mL^{-1}	NA	[71]
Pt-LIG	Gly	AMP	3.03 µM	10–260 µM	NA	[72]
LIG	pH, Na^+, and K^+	OCP	NA	pH: 4–7 Na^+: 0.1–100 mM K^+: 0.1–100 mM	NA	[73]
µPAD	PAR	AMP	0.046–0.154 mmol L^{-1}	50–5000 µmol L^{-1}	NA	[74]
Pt-AuNPs/LIG/PDMS	DA	DPV	75 nM	9.5×10^{-7}– 3×10^{-5} M	NA	[75]

Abbreviations—AuNP: gold nanoparticle; ACE2: angiotensin converting enzyme 2; ACET: acetone; ALC: alcohol; AMP: amperometry; ARA: aristolochic acid; β-ED: β-Estradiol; BP: phosphorene; CFU: colony-forming unit; Chi: Chitosan; CQL: Clioquinol; DA: dopamine; DLEG: Direct Laser Engraved Graphene; DNN: Dense Neural Network; DPAdSV: differential pulse adsorptive stripping voltammetry; DPASV: differential pulsed anodic stripping voltammetry; DT: decision tree regressor; EIS: Electrochemical impedance spectroscopy; ECL: electrochemiluminescence; eMoS_x: electrodeposited molybdenum polysulfide; f-MWCNT: COOH functionalized multiwalled carbon nanotube; Gly: Glyphosate; GLU: glucose; HYD: hydrazine; h-BN: Hexagonal boron nitride 2D material; IPA: isopropanol; LDA: linear discriminant analysis; LIG: Laser-induced graphene; LAC: lactose; LEG: laser engraved graphene; LIG-IDE: laser-induced graphene interdigital electrodes; LIPG: laser-induced porous graphene; LSG: Laser-scribed graphene; LSV: linear sweep voltammetry; LSSVM: least squares support vector machine; MH: maleic hydrazine; MIP: Molecularly imprinted polymers; miRNA: microRNA; NA: not available; NAA: α-naphthalene acetic acid; NFT: nitrofurantoin; N-LSG: nitrogen-doped laser-scribed graphene; Nit: nitrite; NP: nail polish; PAR: paracetamol; PCA: principal component analysis; PLS: partial least squares; PRX: paraoxon; ROX: roxarsone; S1: SARS-CoV-2 spike protein 1; S2: SARS-CoV-2 spike protein 2; SA: salicylic acid; SGN: sulfur doped carbon nitride; SMZ: sulfamethoxazole; SWASV: square wave anodic stripping voltammetry; Ti_3C_2-MXene: graphene-like titanium carbide MXene; TRB: thrombin; TYR: tyrosine; UA: uric acid; ZVO: 3D zinc vanadate.

5.2. Data Analysis Technology

Machine learning (ML) algorithms can optimize the data analysis of complex samples and are well-suited for automating problem solving, based on supervised or unsupervised methods [79]. They can be combined with responses generated by LSG electrodes in diverse environmental, food, and biomedical fields for rapid and maximized analysis, as one can see in Section 6.5 [19,47,79]. The supervised method makes a relationship between dependent and independent variables to predict the future value of the dependent variable according to a dataset. On the contrary, unsupervised learning operates with unlabeled data and groups them by structural similarities [79]. Moreover, supervised learning is subdivided into regression and classification; the first predicts the concentration of the unknown compound (for instance: future blood glucose concentration based on previous measurements [20]), and the second identifies the chemical (for instance: identifying cancer and non-cancer patients using breath sensors [20]) [79]. Therefore, the ML algorithms are trained to make decisions based on the training dataset, so it is necessary to feed them with high-quality data [20,79]. The more information, the better the performance of the algorithms [79]. The training stage is divided into two phases: data pre-processing and model training. The data obtained by a particular sensor are compiled raw, without processing. Afterward, they undergo a pre-processing stage, in which they are standardized and undergo other types of treatment. Then, the most representative data that can provide helpful information for the development of the model should be selected. They can be manually selected by an expert or extracted by an ML algorithm. They are then recompiled into subsets of data for testing, training, and validating the smart model [20]. After briefly describing the importance of generating datasets for creating an intelligent model, we describe the algorithms used for sensing using LSG electrodes.

5.2.1. Artificial Neural Network

Artificial neural network (ANN) or neural network, in short, is widely used today to analyze hidden non-linear relationships; it simulates biological neural behavior. Thus, the method comprises input, hidden, and output layers. It possesses a matrix of interconnected logical computation nodes (compared to artificial neurons) that are separately activated by mathematical functions and weights established by sample data sent into the ANN, which vary from 0 to 1. For instance, functions based on the sum of the interconnecting nodes, such as hyperbolic tangent or logistic sigmoid, could activate nodes when a specific threshold is reached. Alternatively, the weights and biases in each neuron in the hidden layer can be manipulated [20].

5.2.2. Support Vector Machine

A support vector machine (SVM) is a non-neural network algorithm that solves binary classification problems but can be configured to solve multi-classification problems by mapping one input to many classification results [20]. The SVM approach calculates the most significant separation among the input datasets by finding a hyperplane and transforming them into different classes [20,79]. The hyperplane divides the input vectors into linear and non-linear groups with the kernel function. The limiting distance between the hyperplane divider and the input vectors is called the margin. The greater the margin distance between groups, the more accurately the datasets can be classified to improve predictor properties [20,80].

5.2.3. Decision Trees

The decision-making process in decision trees (DTs) is organized in a tree-like structure; it improves the decision criteria at each branching point to classify an information point based on its characteristics [20,79]. The root node is the highest-level decision node representing the entire dataset population. In turn, the root node divides the dataset into lower-level decision nodes (branches) representing part of the dataset's features. These subdivide the features until they can no longer be separated (leaf). A threshold is calculated

at each decision node to divide the most commonly found resources proportionally, based on the Gini Impurity metric [20].

6. LSG-Based Electrodes—Applications to Chemical and Biochemical Sensing

6.1. Environmental Monitoring

Pesticides are synthetic or natural chemicals or mixtures thereof used to control, reduce, or prevent weeds, diseases, and pests that affect vegetable growth [81]. An LSG sensor was used for rapid detection of neonicotinoid pesticides without needing electrode chemical/biological modification on agricultural runoffs and along watersheds aiming to help make guideline policies about the usage of pesticides at a given time and place (Figure 5A) [14]. Neonicotinoids, including imidacloprid (IMD), thiamethoxam (TMX), clothianidin (CLO), and dinotefuran (DNT), act by affecting the acetylcholine neurotransmitter controlling a range of sucking and chewing pests that spoil croplands, home yards, and golf courses. Nevertheless, extensive usage has affected non-target organisms, including various aquatic species, birds, and honeybees. The long-term effects on humans and ecosystems are still inconclusive, due to inadequate appraisal of exposure to neonicotinoids. The sensor showed promise exhibiting low LOD of 823 nM, 384 nM, 338 nM, and 682 nM for CLO, IMD, TMX, and DNT, respectively, suitable reproducibility and no significant interference from broadly used pesticides and herbicides, such as parathion, paraoxon, fipronil, glyphosate, atrazine, dicamba, and 2,4-dichlorophenoxyacetic acid. The LSG sensor responded linearly in a concentration range of 10−40 μM and presented recoveries of 91.8−108.5% in river water.

Organophosphorus (OP) compounds are another group of chemical pesticides widely used in agriculture, veterinary medicine, industry, horticulture, and homes. Poisoning with these substances is an important health problem in the world [82,83]. These compounds are inhibitors of cholinesterase enzymes, which, by phosphorylating the serine amino acid in the active site of the enzyme, create a strong and irreversible bond with the enzyme. By inhibiting the enzyme, they increase the level of acetylcholine, leading to cholinergic crisis, convulsions, and, in severe cases, brain damage and death [84]. Paraoxon is a product of the oxidative metabolism of parathion, which is considered one of the most toxic pesticides. The severity of acute poisoning of this organophosphorus is important compared to other factors, and, despite the prohibition of the use of this organophosphorus, it unfortunately continues to be widely used [85].

In recent research, the determination of the exact values of Paraoxon was followed using a LSG electrode established on a PI foil [67]. First, under well-controlled conditions, the LSG electrode was produced by a laser. Then, the surface of the working electrode was modified with AuNPs through electrodeposition, fulfilled by cyclic voltammetry (30 cycles) in a potential range from −0.9 to −0.1 V and a scan rate of 50 mV s^{-1}. In order to enable signal amplification, a paper modified with MnO_2 nanosheets, conjugated with a DNA sequence (assistant DNA), and a hairpin DNA sequence immobilized on the surface of the electrode was used. The ends of the hairpin DNA sequence were functionalized with thiol for covalent bonding on the surface of AuNPs and ferrocene as the redox marker. The hydrolysis of acetylthiocholine (ATCh) to create thiocholine is often catalyzed by Acetylcholinesterase (AChE) which occurs in the absence of the analyte. This event promoted the removal of MnO_2 nanosheets from the assistant DNA that was used as a complementary strand for hybridization with the hairpin DNA sequence. So, the resultant double-stranded DNA opened the pathway for the enzymatic performance of Nt.BbvCI (which is an endonuclease capable to actuate on a double standed DNA cleaving only one strand) which was the reason for releasing the assistant DNA and a part of the hairpin DNA sequence from the surface of the working electrode (Figure 5B). The released sequences contributed to another switch-bridged DNA signal amplification cycle. So, in the absence of the analyte, since the redox marker molecules were included in the released part of the hairpin DNA sequence, the DPV peak current decreased. Conversely, in the presence of the analyte, the enzymatic reaction was blocked, and the assistant DNA did not release from

the MnO_2 nanosheets. So, the hairpin DNA containing the redox marker remained, and the DPV peak current increased, compared to the absence of the analyte. The linear detection range for this signal-on biosensor was from 3 to 4000 ng mL^{-1}, and the calculated LOD was about 1.2 ng mL^{-1}.

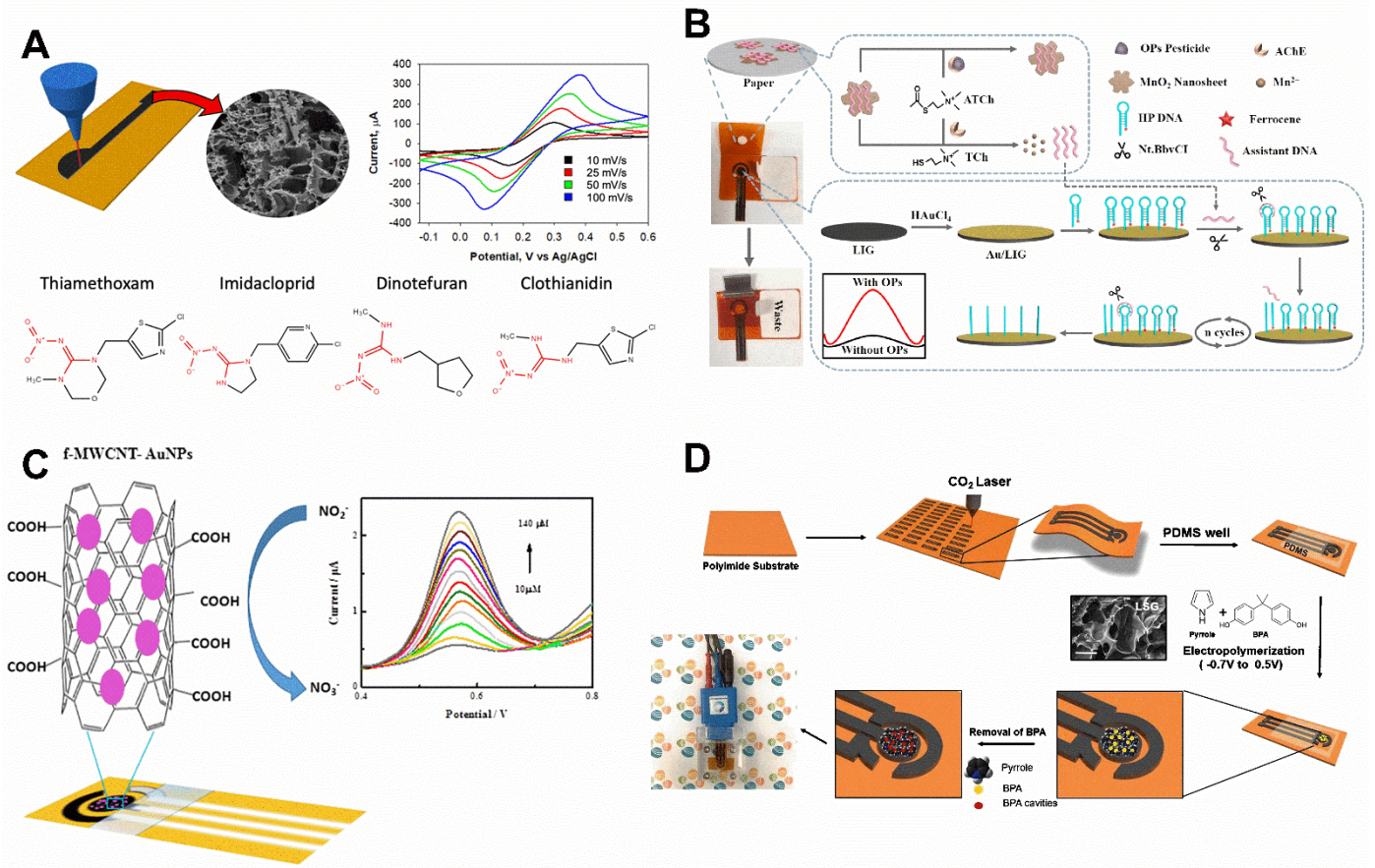

Figure 5. (**A**) Schematic representation of the laser fabrication process of LSG-based electrodes used to detect imidacloprid, thiamethoxam, clothianidin, and dinotefuran. Adapted with permission from ref. [14]. Reuse license received from the American Chemical Society. (**B**) Illustration of the principle of LSG-based electrochemical proposed biosensor based on the MnO_2 switch-bridged DNA signal amplification for the detection of OP pesticides. Adapted with permission from ref. [67]. License Number: 5411960460120. (**C**) Schematic illustration of the NO_2^- electro-oxidation on LSG/f-MWCNT-AuNPs; the inserted figure represents SWV signals of the analyte according to their increasing concentrations that ranged from 10 to 140 µM. [44]. License Number: 5432000551803 (**D**) Graphic demonstration of LSG sensor and MIP fabrication. It was represented the laser engraving process by CO_2 laser on PI substrate, the sensor surface passivation by PDMS tape, pyrrole electro polymerization performed cyclic voltammetry in the presence of bisphenol A, surface cavities on the working electrode after BPA removal, and a picture of the device inside if a PMMA box [32]. License Number: 5432590975732.

In other research, LSG was applied to detect nitrite in water samples. This chemical is employed to preserve processed food to control the development of harmful bacteria. It is also often used as a fertilizer in agriculture, wasting much of it in water and soil. Despite the benefits, it is toxic; it can bind to blood pigments and lead to the production of meta-hemoglobin and, therefore, to a lack of oxygen for the tissues. Moreover, some authors report the fact that nitrite is a potential precursor for the formation of cancer biomarkers, such as aromatic carbenium ions and nitrosamines. Thus, the LSG was modified with COOH functionalized multiwalled carbon nanotube and Au nanoparticles (LSG/f-MWCNT-AuNPs) to synergize electrochemical performance (Figure 5C) [44]. The

synergic effects were evaluated by $[Fe(CN)_6]^{3-/4-}$ redox probes, for which well-defined peaks were observed and the reversible nature of the probes was preserved. It revealed a superior electroactive area, an anodic current density peak about 60% higher, and a peak-to-peak difference of 40% less than the bare LSG. The resistance of charge transfer measured by EIS significantly decreased as well. In an optimized condition (0.1 M PBS, pH 6), anticipation of the oxidation peak and higher current density of the nitrite anodic current was observed. The performance was ascribed to a high specific surface of the LSG sheets, a favorable energy band for the charge transfer of AuNPs to nitrite, its positive surface charge, provided by the cationic polymer layer that favored by the electrostatic attraction, and to the MWCNT's superior conductivity and surface area. The proposed sensor responded to nitrite in a linear range of 10–140 µM and showed an LOD of 0.9 µM. The sensor so prepared presented good selectivity toward 100-fold excess of UA, AA, Cl^-, $NO_3{}^-$, $SO_4{}^{2-}$, K^+, and Ca^{2+}, satisfactory reproducibility with RSD of 2.80%, and the sensor response did not change significantly during seven consecutive SWV runs (RSD: 2.63%).

Likewise, to detect nitrite, nail polish was used as a precursor of LSG using a 405 nm laser. The LSG electrodes modified with chitosan possessed high conductivity, useful mechanical properties, tunable composition, and electrochemical activity. The sensor showed a sensitive and selective response with an LOD of 0.9 µM and a linear range of 2.0–1000 µM. Additionally, the same material doped with copper allowed the detection of non-enzymatic glucose [5].

A flexible LSG electrode with nano-flakes-like and porous morphology was applied to detect hydrazine by cyclic voltammetry (CV). The analyte is widely used in pharmacological, military, aerospace, and energy applications. Nevertheless, hydrazine is neurotoxic and fatal for human health, even in relatively small amounts. For this reason, an LSG electrode was applied to sense hydrazine [45]. The LIG showed a considerable electrocatalytic property for hydrazine in an alkaline solution, due to the electrode elevated surface area and edge defects; as a result, high sensitivity for hydrazine was noticed. The device showed a low LOD and it also did not present any significant interference of glucose, formaldehyde, or AA. The developed electrode also showed good stability, retained 70% of the anodic current after 100 CV cycles, and no signal decrease was reported after 500 bending procedures, proving it to be a flexible sensor.

MIP-modified LSG can be applied to determine bisphenol A (BPA) present in commercial plastics, bottles, and water. This chemical interferes with the production of hormones and is a potential generator of future illnesses, such as those of the breast and prostate, and heart disease [32]. Thus, an LSG device was modified with imprinted polypyrrole with BPA as a template to develop an electrochemical sensor (Figure 5D). It achieved an LOD of 8 nM and a linear calibration range of 0.05–5 µM. Moreover, it displayed high selectivity regarding BPA, compared to its structural analogs, and good reusability. The sensor produced good stability for 15 days but after 20 days its response dropped by 10.3%. Furthermore, it was applied to detect BPA in tap, mineral water, and plastic samples [32].

Laser scribing allows 3D porous graphene frameworks to be produced in a one-step and cost-effective way using PI to modify a conventional glassy carbon electrode (GCE) [46,49]. By mixing Fe_3O_4, MWCNTs, CS, and in-situ plating BF, a novel nanocomposite with remarkable electrochemical performance was obtained for simultaneous and selective detection in trace levels of Cd^{2+} and Pb^{2+} in tap water using SWASV. Heavy metals are highly toxic and bioaccumulate through the food chains. According to the World Health Organization (WHO), the tolerances of Cd^{2+} and Pb^{2+} in drinking water are 3 and 10 µg L^{-1}, respectively [46]. Thus, the composite afforded a fast electron transfer rate and larger effective surface area, thanks to the synergistic effect among the large area of the LSG, the high conductivity of MWCNTs, the adsorption ability of Fe_3O_4, and the outstanding catalytic capability of BF. In this way, the proposed sensor reached an LOD of 0.1 and 0.07 µg L^{-1} for Cd^{2+} and Pb^{2+}, respectively, and a linear range from 1–200 µg L^{-1} for both metallic ions. The sensor's employment in tap water analysis showed its potential applicability in water sample assays providing satisfactory recoveries (97.86–105.96%) and good agreement with analyses made

using atomic absorption spectroscopy. The sensors exhibited long-term stability over four weeks and good repeatability (3.77% for Cd^{2+} and 0.97% for Pb^{2+}) and reproducibility (7.16% for Cd^{2+} and 6.81% for Pb^{2+}).

In another work, GCE was modified with bismuth film and a multilayer of stacked graphene nanosheets produced by the laser-scribed method on the PI. Their great specific surface and many edge-plane active sites facilitated the accumulation of metal ions, such as Cd(II) and Pb(II). The sensor conferred a suitable response for the simultaneous determination of Cd(II) and Pb(II) by means of SWASV, a wide linear range (from 7 to 120 μg L^{-1}), and a low LOD of 0.47 μg L^{-1}. The sensor was applied to the simultaneous determination of Cd(II) and Pb(II) in spiked water samples [49].

Three dimensional-printed electrodes treated with laser scribing were also used for heavy metal detection. Three-dimensional printing is a type of additive manufacturing for rapid prototyping, in that a constructed object acquires a three-dimensional form by adding successive layers. The 3D printer conductive filament consists of a mixture of conductive and non-conductive thermoplastic materials that spoil the electrochemical performance. Costly, non-environmentally friendly, time-consuming, laborious treatments are used to remove them to expose electroactive sites [37]. Thus, Rocha and Ataide et al. proposed a sub-minute (50 s) and reagentless CO_2 laser-scribing treatment to eliminate the insulating polymers from carbon-black(CB)/polylactic acid (PLA)-based 3D-printed electrodes to expose the conductive carbon material, and to create porous-like structures which promote more meaningful interaction at the electrode/solution interface (Figure 6A) [37]. The electrochemical performance toward catechol (CAT), ascorbic acid (AA) uric acid (UA), paracetamol (PAR), $[Ru(NH_3)_6]Cl_3$, and ferri/ferrocyanide redox couple was significantly enhanced when it was compared to the non-treated electrode. A well-defined and lower peak-to-peak separation was obtained. As a result, the sensor allowed enhanced signals for simultaneous determination of Cd^{2+}, Pb^{2+}, and Cu^{2+} with LODs of 1.34, 1.32, and 0.31 μg L^{-1}, respectively. A linear range of 25–125 μg L^{-1}, for PAR quantification in seized cocaine with good recovery was obtained.

Alternatively, Mendes et al. used phenolic papers, a resilient, cheap, and non-conductive commercial material comprised of wood fibers, as an alternative for local pyrolysis by laser scribing, due to better physical and mechanical resistance and stability than papers during analysis (Figure 6B) [38]. The resulting LSG electrodes could be promptly used as electrochemical transducers; nevertheless, they were subjected to electrochemical treatment to enhance electrochemical properties, which provided great conductivity and low charge transfer resistance [38]. The electrodes afforded lower ΔE_p and R_{ct} than the electrochemically untreated electrodes. Furthermore, it provided lower LOD (0.094 μmol L^{-1}) for β-estradiol hormone than the GCE (12.1 μmol L^{-1}). The process of fabrication using phenolic paper revealed good reproducibility and repeatability with RSD of 4.9% (n = 10) and 2.8% (n = 50), respectively.

Polyetherimide (PEI) is a novel polymeric substrate used for LIG sensors. It provides a highly porous carbonaceous material with excellent electrochemical properties for application to the simultaneous detection of emerging pollutants (e.g., hydroquinone (HQ), paracetamol (PA), and methylparaben (MP)) in tap and lake water (Figure 6C) [13]. Electrochemical characteristics, such as heterogeneous electron transfer rate constant (k°, 3.20×10^{-2} cm s^{-1}), the peak-to-peak difference (56.3 ± 8.9) mV, and charge transfer resistance (89 ± 8) Ω, achieved in $[Fe(CN)_6]^{3-/4-}$ stood out from those obtained using LSG on phenolic paper and PI. It became an alternative material to be applied as a disposable and field-deployable electrochemical sensor. Furthermore, it provided an electroactive area 3.4-fold higher than the geometric area and recoveries between 93.1–118%, with LOD of 9.42×10^{-8}, 3.23×10^{-7}, and 2.95×10^{-7} mol L^{-1} for HQ, PA, and MP, respectively.

Other studies have demonstrated valuable efforts to develop analytical methods using LSG sensors for environmental surveillance. A hexagonal boron nitride-modified LSG electrode integrated into a smartphone through Bluetooth to build a wireless platform for outdoor sensing of sulfonamides was developed (Figure 6D) [48]. A platinum-decorated

LSG modified with flavoenzyme (glycine oxidase) was developed for the selective quantification of glyphosate using amperometry in a complex fluid, such as crop residue and river water [72].

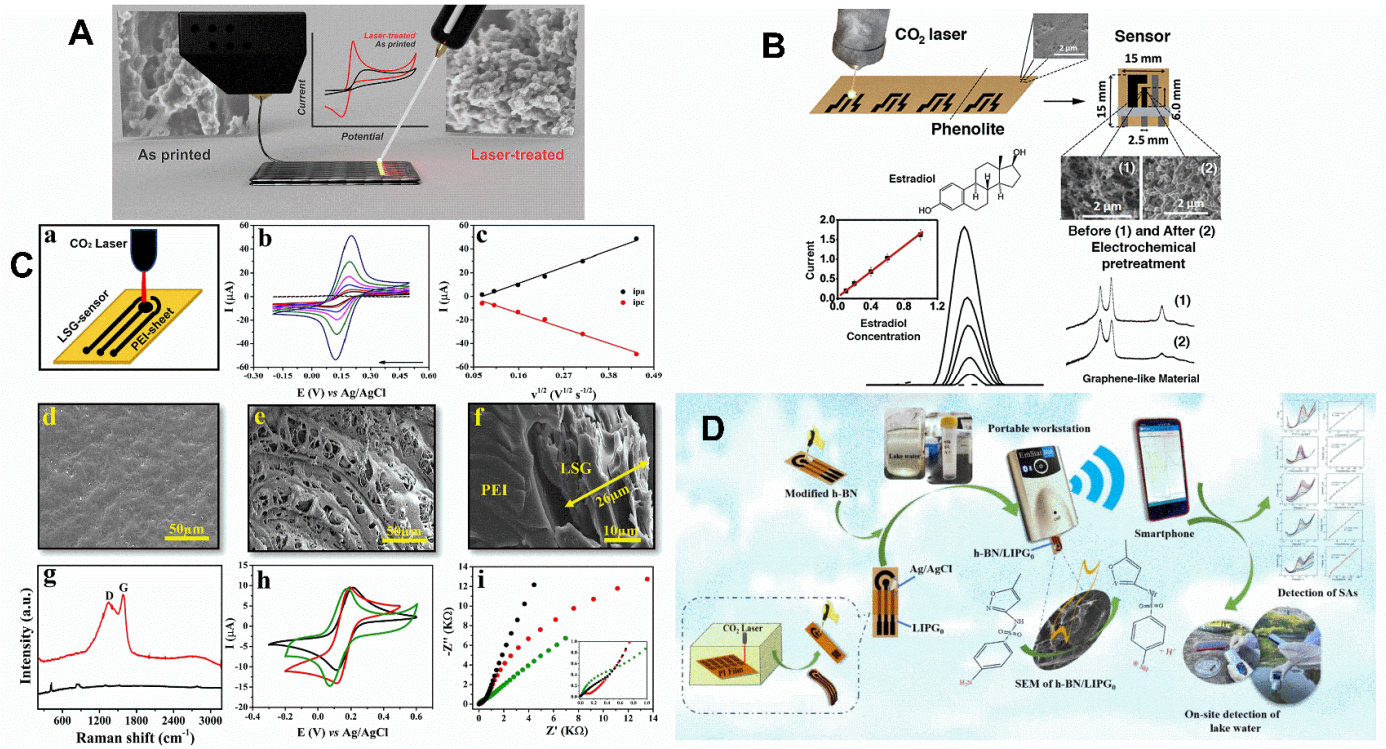

Figure 6. (**A**) Schematic representation of laser treatment of 3D-printed CB/PLA electrodes to improve electrochemical performance. Adapted with permission from ref. [37]. License Number: 5411970297835. (**B**) Manufacturing process and dimensions of the LSG electrode phenolic paper. Raman spectra of the laser-carbonized phenolic paper and electrochemically treated laser-carbonized material. DPV for different estradiol concentrations [38]. License Number: 5432591250600 (**C**) (**a**) PEI-LSG manufacturing schematic representation. (**b**) CVs were recorded with different scan rates (5–200 mV s^{-1}) using the PEI-LSG electrode in KCl solution containing $Fe(CN)_6^{3-/4-}$. (**c**) Anodic and cathodic peak currents as a function of the square root of scan rates. (**d**–**f**) Scanning electron micrograph images with different magnifications of the PEI-LSG electrode. (**g**) Raman spectra of (black) untreated and (red) laser-treated PEI substrate. (**h**) CVs were recorded using LSG electrodes made in different substrates such as (black) PI, (red) PEI, and (green) phenolic paper in a KCl solution containing $Fe(CN)_6^{3-/4-}$. (**i**) Impedance spectra obtained under the same conditions as in item h; the inset represents the enlarged view of the spectra in high-frequency regions [13]. License Number: 5432001490412 (**D**) Graphic illustration of the hexagonal boron nitride-modified LSG electrode preparation and its integration to a smartphone-based wireless platform for portable and rapid detection of sulfonamides [48]. License Number: 5432010230081.

6.2. Food Safety

Direct laser writing was applied to produce a single-use and label-free electrochemical immunosensor to detect *Salmonella enterica* serovar Typhimurium in processed food to mitigate food-borne illness affecting millions of people annually [15]. The LIG sensor afforded low-cost and rapid detection that food industries might employ before the food reaches the consumers. The sensor did not need sample preconcentration and provided a simple detection method. It is an alternative to time-consuming processing and methods requiring highly skilled personnel (e.g., bacteria plate counting and polymerase chain reaction). *Salmonella* antibodies were directly immobilized via EDC/NHS chemistry on the LSG sensor. Detection of *S. enterica* in pristine buffer and chicken broth was assessed

with EIS, and variation in the R_{ct} was proportional to the bond of bacteria on the electrode. The developed biosensor responded in 22 min (consisting of incubation time and EIS measurements) and achieved a wide linear range (25 to 10^5 CFU mL^{-1}), a low LOD (13 ± 7) CFU mL^{-1}, and good selectivity against five other food-borne pathogens, namely *E. coli*, *P. aeruginosa*, *B. cereus*, *S. aureus*, and *L. monocytogenes*.

In another work, a wearable finger electrochemical sensor was fabricated using PI to detect antibiotics used (in many cases in great excess) as additives in livestock breeding to improve growth and low-fat meat [1]. Chloramphenicol, Ractopamine, and clenbuterol, the last two being known as β_2-adrenergic agonists, are contained in lean meat powder and show potential risks to public health in long-term consumption causing human cardiovascular and nervous system diseases. By directly touching samples of pork and milk with fingertips, the developed sensor allowed the rapid detection of antibiotics in the field (Figure 7A) [1]. The proposed device was developed on the PI with working, reference, and counter electrodes integrated and attached to disposable blue nitrile gloves. Then, the electrode surface was covered with gelatin hydrogel prepared in PBS to enable electrochemical measurement. The sensor showed good selectivity. Even though interfering compounds, such as ascorbic acid, uric acid, and dopamine, presented anodic responses, the peak potentials differed from the analytes; thus, they did not interfere with the assays.

Another LSG sensor for antibiotics was developed on PI. The LSG was modified with flower-like $Zn_3V_2O_8$/sulfur doped carbon nitride (SGN) for selective and simultaneous detection of nitrofurantoin (NFT) and chloramphenicol (CAP). Exploring the ZVO/SGN/LSG sensor and the DPV technique to analyze CAP and NFT, a sensitivity of 55.71 μA μM^{-1} cm^{-2} and 23.06 μA μM^{-1} cm^{-2} was reached. The LOD was calculated as 1.5 nM and 2.4 nM, respectively. To validate the use of the sensor in real sample applications, detection experiments were successfully performed on bovine serum and urine [50].

6.3. Health Monitoring

If a person has diabetes, it is essential to monitor the blood sugar level; keeping blood sugar within the standard range can help prevent adverse effects in the future. When sugar is not controlled, complications from diabetes include heart disease, kidney disease, and vision problems [86]. In another study, a novel flexible electrode modified with homogenous Co_3O_4 NPs embedded in 3D porous LSG (Co_3O_4 NPs-LSG) was used to determine different glucose concentrations (Figure 7B) [68]. Due to the highly conductive LSG and many high activation sites of Co_3O_4 NPs, which could improve charge transfer and elevate glucose sensing efficiency, the electrode demonstrated the desired synergistic effect in aiming to detect the analyte. The electrochemical characteristics of the Co_3O_4 NPs-LSG biosensing platform were measured using a standard three-electrode system in an alkaline electrolyte to evaluate potential catalytic performance for glucose oxidation via the amperometry technique. By continuously adding a set of glucose concentrations in an alkaline electrolyte at the desirable potential of +0.55 V, the findings indicated a normal constant amperometric response of the presented Co_3O_4 NPs-LSG biosensor, and a clearly amperometric response pattern was observed. The current abruptly surged when the glucose solution was introduced, and it tended to stabilize rapidly. The Co_3O_4 NPs-LSG biosensor furthermore demonstrated a rapid amperometric response, taking just 0.43 s to reach a stationary current density. The presented biosensor detected the glucose in a linear range from 1 μmol L^{-1} to 9 mmol L^{-1}, with a LOD of about 0.41 μmol L^{-1}.

L-AA is an isomer that naturally exists in many foods and is considered one of the forms of vitamin C. This vitamin is essential for human life and many other living organisms. Vitamin C deficiency can cause scurvy, which was very common in the past among sailors going on long sea voyages [87]. Vitamin C is a food additive and supplement because of its antioxidant properties. Excess vitamin C in the body increases the amount of oxalate, which is excreted through the urine. In some cases, it may stick to minerals causing the formation of crystals that can form kidney stones. Thus, a novel flexible and wearable LSG biosensor, using a combination of $NdNiO_3$ nanotubes (NNO NTs), was proposed for

the non-enzymatic and noninvasive sensing of L-AA [70]. Here, mesoporous aluminum oxide substrates were wet pores filled to create 1D nanostructures of NNO. They were first created on a rigid framework at 700 °C for 8 h in an O_2 environment. Their diameter ranged from 20 to 150 nm. This method of preparation of the material produced consistent 1D $NdNiO_3$ nanostructures with unique morphologies. The oxide formation created the NNO NTs with a dominant alignment and a homogeneous crystalline structure on the L-ascorbic acid templates. Both GO/NNO20 and GO/NNO100 wearable sensors were created as prototypes and tested to see how well they worked at detecting analytes. The GO/NNO nanosensors were also employed in the simultaneous detection of actual samples to fulfill all the requirements for the proposed platforms. As a result, both prototypes offered the requisite recovery time and could identify L-AA in artificial sweat. These biosensors demonstrated sufficient sensitivity, stability, and specificity during L-AA detection. They could detect the analyte in a wide range, between 30 and 1100 μmol L^{-1}, with a determined LOD of around 3.8 μmol L^{-1}.

Dopamine (DA) is a neurotransmitter fundamental in the nervous system, responsible for transmitting messages between nerve cells. Too much or too little dopamine can lead to severe health problems, such as Parkinson's disease [88]. In an interesting research, the integration of poly(3,4-ethylenedioxythiophene) (PEDOT) as a conductive polymer with LSG introduced a sensing application for dopamine [56]. Here, a LSG working electrode with 2 mm diameter was produced through laser process in an optimized condition. Afterward, the surface of the LSG electrode was modified with a layer of PEDOT through electrodeposition (chronoamperometry: 1.2 V for 15 s). The electrochemical characterization confirmed that this modified electrode had a surface area of 0.2 cm^2, corresponding to a roughness factor of 6.36. The detection of dopamine was followed via the DPV, and the presented sensor detected the analyte in a linear range from 1 to 150 μmol L^{-1}, and the reported LOD was 0.33 μmol L^{-1}.

Likewise, DA was detected using laser-scribed commercial carbon SPE using DPV in the presence of an excess of typically found interfering agents, such as AA and UA [89]. Contrary to most investigations that report the creation of carbon structure defects by laser treatment, the benefit of the CO_2-laser thermal action in ambient conditions increased graphite crystallinity, verified by decreasing the D/G Raman bands ratio [89]. Indeed, it improved the electron transfer rates and enabled simultaneous identification of AA, DA, and UA. Furthermore, the laser treatment favored introducing oxygen groups by anodization to improve the detection of substances, such as DA, that are sensitive to oxygen on the surfaces (Figure 7C). Likely, the thermal action removed the excess binders and impurities and burned small graphite particles and less crystalline graphite, exposing the pristine graphite surface, which is much more reactive, facilitating electrochemical oxidation, compared to the untreated SPE. Therefore, the combination of the treatments improved the resolution of the oxidation peaks of the three substances in comparison to the untreated electrode. Linear response from 0.34 to 1.6 μM and a low LOD of 80 nM were observed. The proposed sensor responded after ten days of storage, at least in vacuum-packing. In another work, Hui et al. developed a highly flexible electrochemical sensor based on a Pt–Au nanoparticles (Pt-AuNPs)-modified LSG transferred to Polydimethylsiloxane (PDMS) for selective detection of DA among UA and AA in human urine. The device provided high electrocatalytic activity in response to the oxidation of DA and defined DPV current peaks with a separation of 0.11 V for DA and UA [75].

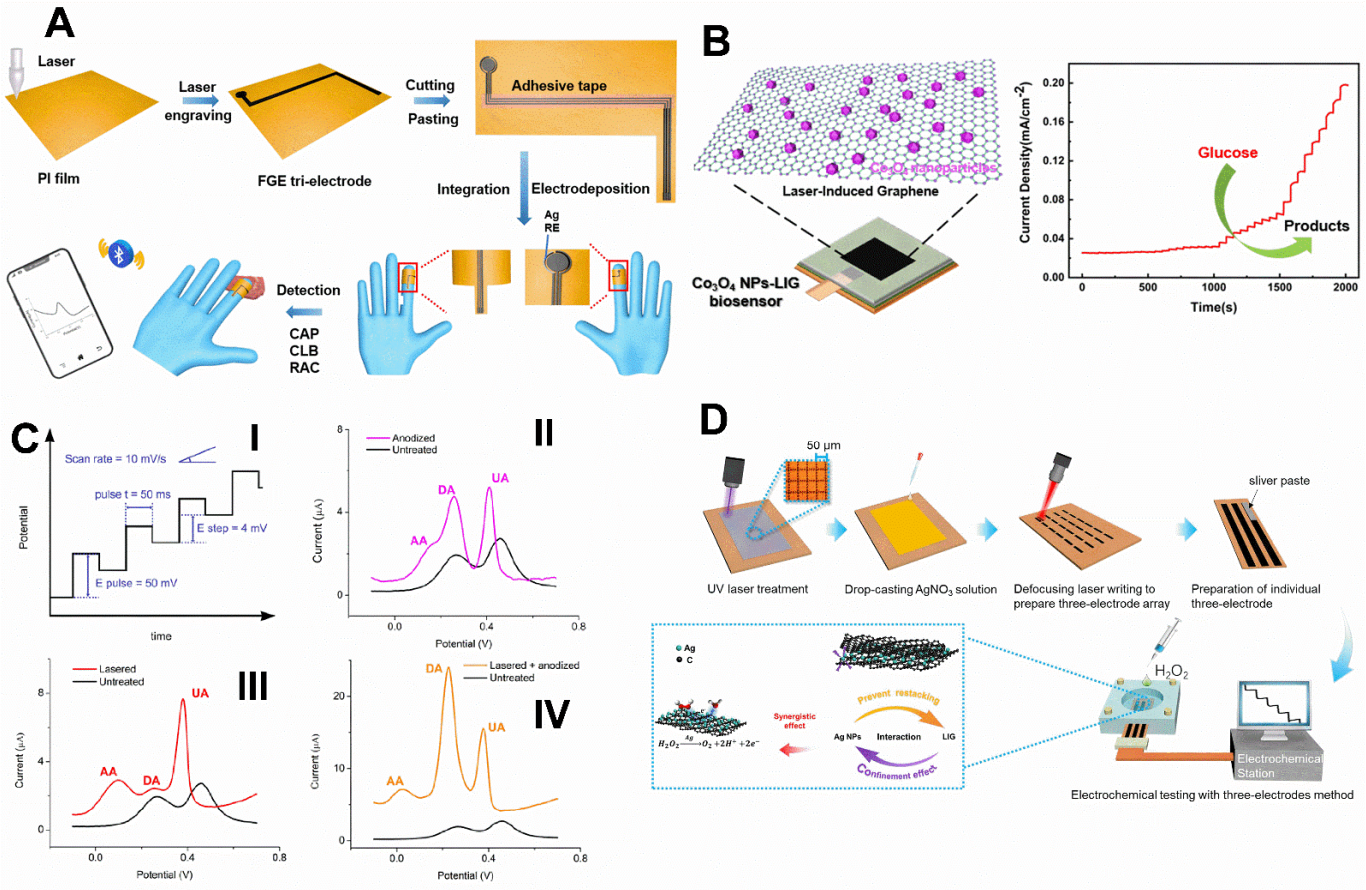

Figure 7. (**A**) Graphic illustration of finger LSG flexible electrochemical detection system to detect chloramphenicol (CAP), ractopamine (RAC), and clenbuterol (CLB) in pork and milk. Adapted with permission from ref. [1]. License Number: 5411970964877. (**B**) A representation illustration of a manufactured flexible Co_3O_4 NPs-LSG sensor and its amperometric response to glucose with several concentrations at an applied potential of +0.55 V [68]. License number: 5432031071827 (**C**) (**I**) DPV parameters used to yield the best analytical response at these electrodes. (**II**) DPVs of AA, DA and UA in 0.1 M PBS pH 4 at untreated (black), anodized (pink), (**III**) lasered (red), and (**IV**) lasered-anodized (orange) commercial carbon SPEs. All the voltammograms were obtained against Ag pseudo-reference electrode. Adapted with permission from ref [89]. License Number: 5411980160451. (**D**) Schematic diagram of the fabrication and application of the LSG@Ag electrode on hydrogen peroxide sensing. Adapted with permission from ref. [35]. License Number: 5412001392675.

UA is produced by breaking down purines. Purines are nitrogen-containing compounds in body cells, including DNA [90]. The UA medical test measures the amount of this substance in blood or urine. As cells age, they break down and release purines into the blood. If UA is produced in excess, it can accumulate in the body and cause an increase in its blood level (hyperuricemia). Excess UA can cause gout, a condition characterized by inflammation of the joints due to the formation of UA crystals in the joint (synovial) fluid. Excess UA can also accumulate in tissues such as the kidneys, leading to kidney stones or kidney failure. In another study, gold clusters and chitosan were used to create a chitosan–Au–LSG electrode with hydrophilic property and a conductive 3D graphene sheet. The new way of tailoring this electrode resulted in high performance of the sensor, which presented excellent performance for use in vitro and in vivo environments. It was demonstrated that the same sensor could be used for the detection of UA and pH simultaneously [73]. Here, the essential procedures included electrodeposition of Au clusters to modify the LSG's surface and coating the signal transducer's surface with chitosan, aiming to construct a super hydrophilic surface without endangering the LSG's porous structure. The CVs peak

current related to the modified LSG electrode with the Au and chitosan confirmed the improved surface of LSG (chitosan–Au–LIG). The specific structure of chitosan–Au–LIG also displayed an antifouling capability in bovine serum albumin (BSA) and bovine plasma medium via the same method. Furthermore, the chitosan–Au–LIG electrode exhibited the required performance in sensing UA and pH through the DPV technique. Using the developed platform of the chitosan–Au–LIG wearable biosensor, it was possible to monitor the amount of uric acid in human sweat over about 10 days, which might serve as a proxy for purine consumption. The analyte was determined with the electrochemical sensing platform and demonstrated an LOD of about 0.5 μmol L^{-1}.

Hydrogen peroxide (H_2O_2) chemistry is widely used in daily life, most notably in food handling, bioprocess, medical cleansing, and medical care, among other applications [91]. Its level is a strict indication for several biological and industrial purposes, which call for precise and prompt monitoring. Reactive oxygen species (ROS) abnormally secreted by the body, such as H_2O_2, can harm cell components and result in heart attacks, Alzheimer's, Parkinson's, and cardiovascular disorders. In an important research, a quick approach for making silver nanoparticle-anchored LSG electrodes (LSG@Ag) was developed for determining various concentrations of hydrogen peroxide (Figure 7D) [35]. The synthetic LSG@Ag electrodes reflected a laminar structure with flaws and micropores, which might offer many active sites for binding the AgNPs with the desired hydrogen peroxide catalytic performance and enhance the dispersion ability. Remarkably, the LSG and AgNPs had a robust chemical interaction. The spatial confinement effect of LSG might hinder the increase in size of AgNPs, and the AgNPs could also prevent the graphene nanosheets from reorganizing (Figure 6). The reported sensor exhibited two distinct linear detection ranges, the first from 0.01 to 0.55 mmol L^{-1} and a second from 0.55 to 2.61 mmol L^{-1} with an LOD of about 2.8 μmol L^{-1} measured by electrochemical amperometry.

The neurotoxicity drug clioquinol also works as a chelator for zinc and copper. Since zinc and copper are involved in the formation and stability of amyloid plaques and because chelating drugs may remove amyloid accumulations in in-vitro and in-vivo conditions, metal chelation is a possible treatment approach for Alzheimer's disease (AD) [92]. As it lessens oxidation and the amyloid load, clioquinol's capacity to chelate and redistribute metals often plays a significant role in disorders like AD and Parkinson's disease, characterized by Zn, Cu, and Fe dyshomeostasis. Chelators made of zinc may also have anticancer properties. A flexible three-electrode framework for the tracking of clioquinol was described in a study utilizing an LSG electrode as the signal transducer. This transducer consisted of Nafion-Fe_3O_4 nanohybrids employed as a modifier on the surface of an LSG electrode. The counter and the reference electrodes were built on the same polyimide film [69].

By dropping a solution of Nafion-Fe_3O_4 nanohybrids, which, through electrostatic interactions, could be self-assembled into Fe_3O_4 (containing positive charge and Nafion containing negative charge) on the surface of the LSG electrode, the electrode was employed to quantify the clioquinol in biofluids. An improved surface-to-volume ratio was supplied by the uniform dispersion of Fe_3O_4 in combination with the strong electrostatic interaction of Nafion-LSG in a superhydrophobic environment. This improvement on the surface of the signal transducer simplified the process of adapting electrolytes to the electrode surfaces. It provided a quick and accurate electrochemical detection pathway for the analyte molecules. The manufactured sensor had the desired sensitivity and could detect the analyte in a linear range from 1 nmol L^{-1} to 100 μmol L^{-1}, with a reported LOD of approximately 0.73 nmol L^{-1}.

Human sweat contains different biomarkers that attest to the health status of individuals. This includes electrolytes like sodium and potassium, metabolites like lactate and glucose, and small amounts of hormones and peptides. Monitoring these biomarkers is a way to obtain important information about the health of the human body. Thus, an LSG-based wearable sweat sensor was engineered for noninvasive multiplexed ion detection [73]. The ion-selective membranes were added on poly (3,4-ethylene dioxythio-

phene): polystyrene sulfonate (PEDOT:PSS)-modified LSG, and the Na^+ membrane was prepared by blending Na ionophore X, sodium tetraphenylborate (Na-TPB), polyvinyl chloride (PVC), and dioctyl sebacate (DOS); for K^+ ion-selective membrane was mixed valinomycin as an ionophore, potassium tetrakis (4-chlorophenyl) borate (KTClPB), PVC, and DOS; for H^+, polyaniline was electrodeposited. The devices can simultaneously monitor pH, Na^+, and K^+ levels with a sensitivity of 51.5 mV decade^{-1}, 45.4 mV decade^{-1}, and 43.3 mV decade^{-1}, respectively. Ion concentrations can be transmitted remotely and wirelessly to a personalized smartphone app in real-time during the user's physical activity.

6.4. Clinical Diagnosis

The COVID-19 pandemic challenges global public health systems, causing severe damage to lives and economics. Point-of-care (POC) devices are highly needed to control the current pandemic caused by severe acute respiratory syndrome Coronavirus 2 (SARS-CoV-2). While gene expression analysis (e.g., RT-PCR) is broadly available, they require sample preparation and are time-consuming. In this way, an electrochemical immunosensor for COVID-19 diagnosis was developed by graphitizing PI. A gold nanostructure modified with cysteamine was electrodeposited on the LSG to allow the immobilization of the anti-spike protein antibody of SARS-CoV-2 for its selective detection (Figure 8A) [77]. The biosensor was integrated into a handheld, customized point-of-care detection system in association to a smartphone application by USB port; it consisted of multichannel electrochemical devices permitting multiple amperometry and voltammetry assays. It provided a user-friendly platform for diagnosis and systematic data management. The specific antibody–antigen coupling prevented cross-reactivity with immunoglobulin G (IgG), M (IgM), and glycoproteins. A threshold classification was determined statistically to group the samples as positive and negative, and the tests yielded comparable results with the real-time polymerase chain reaction (RT-PCR) assays.

In another work, a four-working-electrode graphene array device was produced to enable detection of COVID-19 in blood and saliva samples. According to the authors, the arrangement was multiplexed, field-deployable, offered friendly usage, was sensitive, rapid, cheap, wireless, and suitable for telemedicine applications. The LSG was generated on PI; it was modified with 1-pyrenebutyric acid (PBA) linker to permit immobilization of SARS-CoV-2 nucleocapsid protein (NP) antibodies, C-reactive protein (CRP), and immunoglobulin capture spike proteins (S1) to detect the SARS-CoV-2 NP antigen, biomarker C-reactive protein that signals inflammation, and IgM/IgG antibodies, respectively [78]. It allowed the early identification of the infection to prevent the spread of the disease by presymptomatic and asymptomatic persons. The proteins and specific immunoglobulins were detected using sandwich- and indirect-based immunosensing approaches. Moreover, the biosensor did not show non-specific reactions with the following: IgGs of SARS-CoV-2 NP and S1, and IgG and IgM against both MERS-CoV and SARS-CoV, in the case of IgG/IgM assays; B-type natriuretic peptide, SARS-CoV-2 NP, SARS-CoV NP, and SARS-CoV S1, for CRP assays; and SARS-CoV-2 S1, SARS-CoV S1, and CRP, for NP assays. However, as expected, interference was noticed when SARS-CoV NP was considered in SARS-CoV-2 NP interference assays because of their high structural similarities (90%). Despite the absence of selectivity, it was not considered a concern regarding the non-emergence of new SARS-CoV cases recently.

Recent research described the successful detection of antibodies. Different types of antibodies are available in body fluids. The body's immune system increases the level of antibodies to protect various organs against bacteria, viruses, allergens, and other possible pathogens. Immunoglobulin G (IgG) is the most abundant type of antibody in blood and other body fluids that protects the body against viral and bacterial infections [93]. The level of this antibody increases in several diseases, such as sarcoidosis and chronic liver diseases, some parasitic infections, chronic infections or recurrent infections, lupus erythematosus (SLE), rheumatoid arthritis, and Sjogren's syndrome. In another investigation, an electrochemical immunosensing platform was designed for the sensitive detection of

IgG based on a modified laser-scribed graphene (LSG) electrode with cationic polyelectrolyte polyallylamine (PAAMI) and PtNPs (Figure 8B) [71]. Through non-covalent π-π interaction and electrostatic physical absorption, PAAMI was employed to stabilize LSG flakes, while preserving the substrate's inherent thermal and electrical capabilities. By providing amino functional groups, the integration of PAAMI gave many clipping areas for the adsorbed molecules, improving the stability of the LSG platform by electrostatic adsorption and the rate of electron transfer. Additionally, the denaturation issue of the immobilized biomolecules was mitigated by the cationic nature of the electrode surface. The presented immunosensing system was utilized to identify immunoglobulin (IgG) in a broad linear range between 0.012 and 352 ng mL^{-1}, with an LOD of about 6 pg mL^{-1}. According to the experimental investigation, the introduced biosensor may be employed for the point-of-care measurement of IgG in diagnosing facilities.

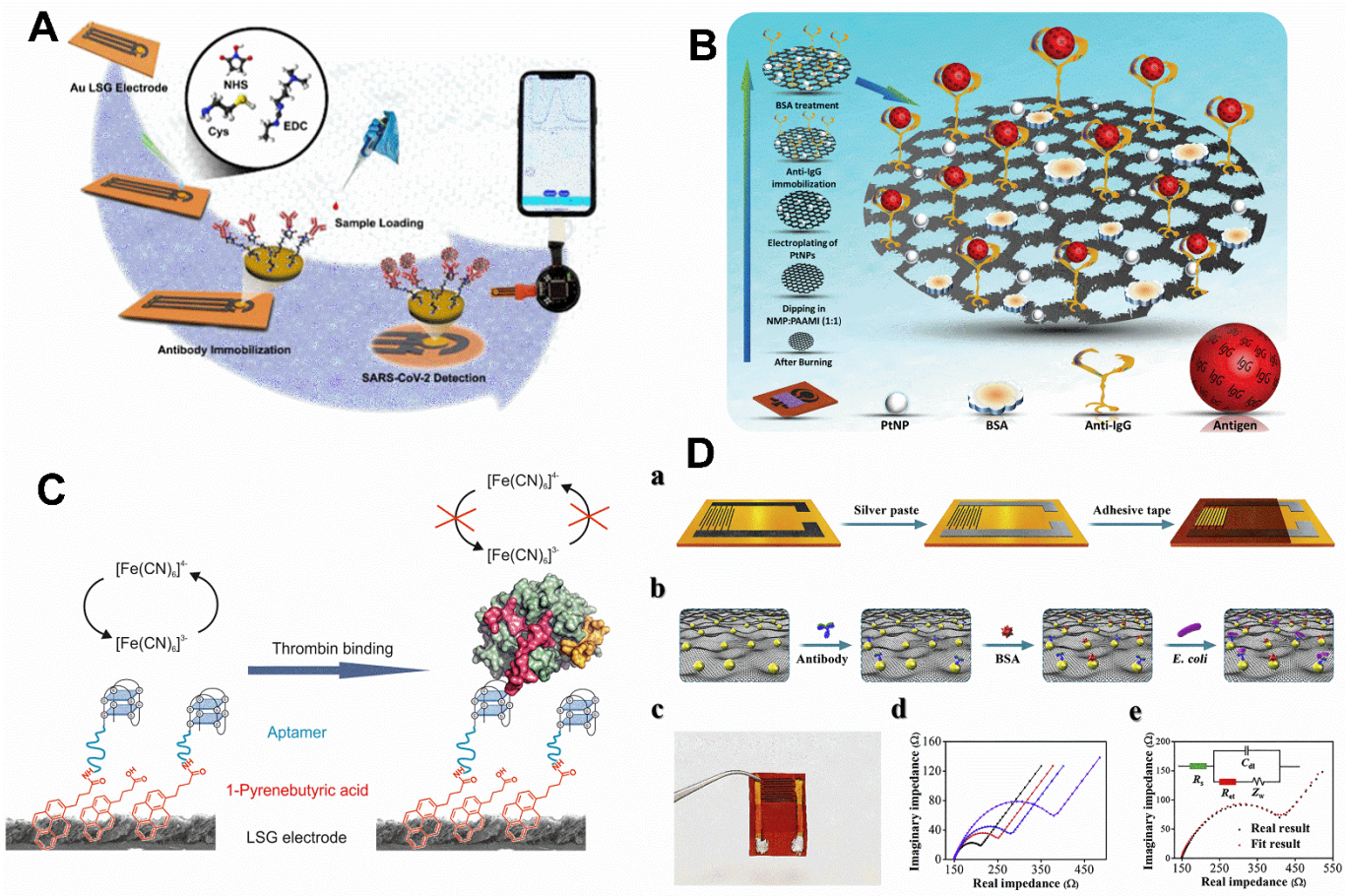

Figure 8. (**A**) Representative of Au LSG modification with antibodies and the detection of SARS-CoV-2. The inset photo is the biosensor integrated into a smartphone by USB port. Reprinted (adapted) with permission from [77]. Copyright 2021 American Chemical Society (**B**) Graphic illustration of the PtNPs/PAAMI/LSG-based immunosensor [71]. License number: 5432031284784 (**C**) Electrochemical mechanism representation of thrombin detection. As the thrombin concentration increased, increasing difficulty the redox mediator was found to diffuse to the electrode surface; this decreased the currents intensities obtained from voltammetry assays. Adapted with permission from [66]. Copyright 2017 American Chemical Society (**D**) (**a**) Representative of the AuNPs-LSG interdigitated array electrode fabrication using single-step laser scribing; (**b**) Illustration of the electrode-based immunosensor for the E. coli detection; (**c**) Photo of the AuNPs-LSG interdigitated array electrode; (**d**) Nyquist plots obtained in each step of electrode modification: AuNPs-LSG electrode (black line), antibody modification (red line), BSA blockade (blue line) and bacteria capture (purple line); (**e**) Nyquist plot fitting curve using the Randles circuit after incubating the electrode with 1×10^6 CFU mL^{-1} of *E. coli* [51]. License number: 5432040094543.

Despite significant advancements in the rapid and accurate identification of proteins in biological samples, several studies are constantly being carried out to enhance these techniques. Thrombin, one of these proteins, is crucial for blood coagulation, clot dissolution, and tissue healing [94]. In addition, thrombin can control platelet aggregation, endothelial cell activation, and other critical vascular biology responses. Therefore, it is crucial to create thrombin detection sensors with excellent sensitivity and selectivity for use in both research and for clinical diagnostic purposes. In another research, an aptasensing platform was introduced to determine various concentrations of thrombin using LSG modified with PBA (Figure 8C) [66]. The use of PBA provided the surface of the LSG electrode functionalized with the carboxyl group, which, through the EDC/NHS linker, was able to join to an amino-functionalized aptamer sequence as the biorecognition element. The electrochemical measurements for the detection of the analyte were performed by DPV, and the principle of detection was based on the electrostatic repulsion interaction that occurred in the presence of various concentrations of the analyte. By increasing the concentrations of thrombin, the access of redox marker molecules decreased, which led to a regular and significant decrease in the DPV peak current, which introduced signal-off behavior. The presented aptasensor could determine various concentrations of thrombin in a linear range from 1 to 100 pmol L^{-1}, and the calculated LOD for this platform was equal to 1 pmol L^{-1}.

Escherichia coli strain O157:H7 is a microorganism transmitted to humans through contaminated food and water. Settling in the intestine, it leads to severe injuries, such as hemorrhagic colitis and hemorrhagic urinary syndrome [95]. Children are the primary victims of the disease. This pathogen results in many yearly reported deaths, especially in children under five. In Escherichia coli strain O157:H7, the gene encoding the O157 antigen is encoded by a 12-gene cluster [96]. Six of these genes are responsible for sugar-base biosynthesis. The protein coded by four other genes is also used to transport sugar. Two other genes also code O-antigen flippase transporter proteins. The protein coded by the rfbE gene is in the group of proteins involved in sugar-base biosynthesis and plays a role in synthesizing bacterial lipopolysaccharide. In research focused on Escherichia coli, several noble metal nanoparticle-3D graphene nanocomposites were made using a one-step laser induction process. The nanocomposites were synthesized from PI film covered with the matching metal precursor's chitosan hydrogel ink. These nanoparticles, which included gold, silver, and platinum, were uniformly dispersed on the surface of porous 3D graphene and were utilized to create an impedimetric immunosensing platform for diagnosing Escherichia coli O157:H7 (Figure 8D) [51]. Here, the electrode substrate was initially coated with chitosan-mediated ink that included a metal precursor on the polyimide sheet. Then, porous metal nanoparticle–graphene nanocomposites were created by laser scanning the metal precursor-modified PI film. The synthesized noble metal nanoparticles were homogeneous and of desired quality on the LSG surface. An AuNPs-porous graphene electrode was also employed for designing an interdigitated array form. In order to set up the immunosensor to identify *E. coli* O157:H7, the antibodies as the biorecognition element were immobilized on the surface of a modified microarray electrode with AuNPs–graphene through an adsorption process between antibodies and AuNPs. The antibody-modified AuNPs–LSG interdigitated array electrode (immunosensor) was exposed to various concentrations of E. coli O157:H7, and the resulting EIS curve for each concentration was recorded. This immunosensor could detect the analyte in a linear range from 1×10^2 to 1×10^8 CFU mL^{-1}.

Moreover, a flexible LSG/Au electrode was developed for label-free detection of oncomarker carcinoembryonic antigen. The LSG electrode was produced using an inexpensive 450 nm semiconductor laser under ambient conditions. Then, the LSG electrode was modified with AuNPs to allow carbonylation through anchoring 11-mercaptoundecanoic acid, followed by covalently bound carcinoembryonic antibodies via EDC/NHS chemistry to build a label-free immunosensor. The immunosensor displayed suitable sensitivity to respond in the low concentrations range, from 0.01–100 ng mL^{-1}, had a low LOD of

5.0 pg mL^{-1}, high selectivity likened with some possible interference and could be utilized in a bovine serum solution without the need for sample pretreatment [76].

6.5. LSG Electrodes Integrated with Machine Learning Models

Machine learning (ML) models can evaluate analytical parameters collected by LSG electrodes to obtain good predictions. They enhance the evaluation of the relationship between peak currents and analyte concentrations. Traditional linear regression generally judges only by R^2. Contrarily in ML models, different statistical criteria can be used to assess the efficiency of modeling. The most used are the determination coefficient of calibration ($R_C{}^2$) and prediction ($R_P{}^2$) set, root mean square error (RMSE) of calibration (RMSEC) and prediction (RMSEP) set, mean absolute error (MAE) calibration (MAEC) and prediction (MAEP) set and residual prediction deviation (RPD) in the prediction set. Zhu et al. discussed the suitable value for each parameter to obtain a well-tuned model [80]. ML overcomes problems like non-linearity or over-fitting (e.g., square roots of analyte concentration), which is required, in some cases, for better linearization.

Thus, fish freshness was intelligently evaluated using an ANN algorithm. LSG flexible nanozyme electrode prepared using a homemade laser-scribing engraver was used to simultaneously detect xanthine (XT) and hypoxanthine (HX) over store times using DPV [47]. The electrode displayed an oxidase-like activity for the quantification of XT and HX, resulting in a LOD of 0.26 μM and 0.18 μM and a linear range of 0.3–179.9 μM and 0.3–159.9 μM, respectively. The low value of the Michaelis–Menten constant revealed that LSG effectively created a binding site in the abnormal–affinity synthetic hollows for the analytes, which suggested an enzyme-like characteristic of the LSG. The nonlinear ANN fitted better than the traditional linear regression to the electrochemical responses in the function of different analyte concentrations, resulting in good prediction for quantifying XT and HX after training detection models grounded on the group of known responses.

A dense neural network (DNN) algorithm was used to automate COVID-19 diagnosis. The algorithm improved and accelerated the reading of responses generated by the AuNP/LSG electrode functionalized with angiotensin-converting enzyme 2 in the biorecognition of SARS-CoV-2 spike proteins (S1 and S2) of different variants. [19] The method could identify alpha, beta, and delta variants with 99.37% accuracy in 1 min in nasopharyngeal swab samples from 63 patients without needing expertise and pre-sample preparation. The sensor was integrated into a home-produced and field-deployable potentiostat connected to a smartphone with a customized application for easy and friendly operation. The sensor's linear range response was 1.0–200 ng/mL and LODs achieved were 5.14 and 2.09 ng/mL for S1 and S2 protein, respectively [19].

LSG sensors were fabricated to selectively detect salicylic acid (SA) [64] and maleic hydrazine (MH) [61] in agro-products by linear sweep voltammetry (LSV) and DPV, respectively. The sensor was coupled to a portable mini-potentiostat with Bluetooth communication with a tablet. [64] The relationship between peak current responses and SA concentrations varied non-linearly, fitting well with LSSVM and ANN algorithms. However, the performance of LSSVM was superior in comparison with ANN for practical applications, due to less drawback from local minimum and over-fitting [64]. MH's responses were divided into different concentration ranges for the best fitting and processed by RF, LSSVM and ANN algorithms. However, ANN and RF prediction abilities were influenced by the concentration range and data range number; thus, LSSVM was the best model for prediction on actual samples [61].

Another chemical present in agro-products, α-naphthalene acetic acid (α-NAA), was detected employing an LSG electrode coated with two-dimensional phosphorene/graphene-like titanium carbide MXene (BP/Ti_3C_2-MXene) [59]. The current response varied linearly with increase in α-NAA concentration; however, it reached a plateau after successive additions. Indeed, it hampered linear analysis affecting preciseness and detection concentration range. ANN improved the dynamic range from 0.02–0.1 μM to 0.02–10 μM and accuracy. The ANN model allowed good prediction of α-NAA concentrations, based on data ob-

tained in the experiment, even where the slope varied non-linearly; it showed suitable performance to be applied in actual samples (e.g., soil, tea, rice, wheat, corn, and water).

7. Conclusions and Perspectives

Laser scribing technology is a relatively new manufacturing process that has shown its great potential in many research directions over the last few years. The advances in the sensing field of LSG electrodes' applications compiled in this review are a result of its outstanding conductivity, efficient electron transfer rate, sizeable available surface area, and facility to modify the surface with nanomaterials, biological molecules, and polymers. They were integrated with data analysis technology to recognize the response patterns for rapid and more precise data analysis to fabricate intelligent devices, and due to their flexibility, it was possible to produce wearable devices. The sensors have been successfully applied in many areas, with emphasis on clinical diagnosis, food safety, and environmental and health monitoring. Indeed, this technology will soon be in a new group of electrochemical sensors and biosensors with thrilling applications.

Even considering the great number of papers published till now, the field is in its infancy. There are plenty of opportunities to extend this research area. The graphene-like structure of LSG is not robust enough and can be peeled off by physical touch or by applying relatively high voltage, deteriorating its electrical properties. The mechanical stability and conductivity of the LSG may be enhanced by its modifications with nanostructures/conducting polymers, doping with highly conducting nanomaterials, or using different gases in the environment during the fabrication process. Studies could be conducted to optimize different modification processes, such as doping of the electrode, and controlling the stability, reproducibility, sensitivity, and selectivity. A combination of treatments could enhance the electrochemical performance. Laser-scribing, followed by electrochemical treatment, proved to be a great way to improve the detection sensibility; however, it is rare and deserves to be more studied.

Another way to explore LSG in sensing is by using MIPs to mimic bioreceptors for selective detection. It can capture small analytes, such as heavy metal ions and organic molecules, to big ones, such as proteins and whole bacteria. Likewise, integrating LSG sensors/biosensors into microfluidic devices for fully automated assays is scarce. In this way, the microfluidic field that allows efficient mass transport, driven by an external pump or capillarity for the promotion of reaction or separation of compounds, could be coupled with electrochemical high-throughput LSG devices. In addition, mass transport efficiency could be exploited using flow-injection and batch-injection analyses for serial and high-throughput analysis. The flexibility of the LSG-based electrochemical sensors and biosensors could be further explored for application in wearable devices. The possibility to engrave LSG on clothes and flexible polymers, or transfer the LSG easily to stretchable polymers, could expand the horizons for more applications in this direction. Integrating LSG smart electrodes with current-generation communication systems or smartphones would enable sharing of data to the monitoring station for remote reading, dismissing the need for the presence of qualified personnel. This would allow recording of point-of-need diagnosis, health monitoring, and analysis of chemicals/microorganisms that threaten health, even in hard-to-reach places.

The development of health self-test devices for real life, like glucometers, is the apple in the eye in the field of portable and disposable sensors. The features of LSG smart electrodes, such as portability, ease of use, stability, and ease of modification, could be allies in their development. The association of the sensors with smartphones and tablets facilitates storage and processing of the data generated by LSG electrodes. Their global positioning system with appropriate monitoring strategies can be used to map riverside regions to quantify toxic metals due to human activities, for instance.

Finally, regarding the sensor fabrication process, the resolution of the laser for engraving the substrates would be improved by using a highly focused laser beam that can steer the high-resolution arrays to design miniaturized multi-analyte sensors or increasingly

smaller sensors to do assays at low sample volumes, optimizing laser scan rate, power, frequency, and output z-distance. Furthermore, it would be attractive to explore different substrates, such as paper, that are biodegradable and of renewable origin, poorly used in this field, to develop electrochemical paper-based analytical devices to apply to chemical and biological sensing. Equally, another minor-used substrate is 3D-printed electrodes, which provide reproducible responses and are automatedly manufactured. It would be highly appealing to use this novel technique to treat/modify the emerging classes of devices.

Author Contributions: All the authors confirm the equal contributions, approve this article's final version, and agree with submission to this journal. The submitted paper is the original work of the authors and has not been previously published, nor is not considered for publication anywhere else. The manuscript is also not subject to any conflict of interest. All authors have read and agreed to the published version of the manuscript.

Funding: The authors acknowledge the financial support from São Paulo Research Foundation—FAPESP (grant numbers: 2019/22126-2, 2018/16896-7, 2017/13137-5 and 2014/50867-3), and from to the National Council for Research—CNPq (processes 311847-2018-8, 465389/2014-7, and 305247/2022-0).

Institutional Review Board Statement: Not applicable.

Informed Consent Statement: Not applicable.

Data Availability Statement: All data presented in this paper are available for all readers.

Conflicts of Interest: The authors declare no conflict of interest.

References

1. Li, J.; Bo, X. Laser-enabled flexible electrochemical sensor on finger for fast food security detection. *J. Hazard. Mater.* **2022**, *423*, 127014. [CrossRef] [PubMed]
2. Nah, J.S.; Barman, S.C.; Zahed, M.A.; Sharifuzzaman, M.; Yoon, H.; Park, C.; Yoon, S.; Zhang, S.; Park, J.Y. A wearable microfluidics-integrated impedimetric immunosensor based on Ti3C2Tx MXene incorporated laser-burned graphene for noninvasive sweat cortisol detection. *Sens. Actuators B Chem.* **2021**, *329*, 129206. [CrossRef]
3. de Araujo, W.R.; Frasson, C.M.R.; Ameku, W.A.; Silva, J.R.; Angnes, L.; Paixão, T.R. Single-Step Reagentless Laser Scribing Fabrication of Electrochemical Paper-Based Analytical Devices. *Angew. Chem. Int. Ed.* **2017**, *56*, 15113–15117. [CrossRef] [PubMed]
4. Chaudhary, V.; Gautam, A.; Silotia, P.; Malik, S.; de Oliveira Hansen, R.; Khalid, M.; Khosla, A.; Kaushik, A.; Mishra, Y.K. Internet-of-nano-things (IoNT) driven intelligent face masks to combat airborne health hazard. *Mater. Today* 2022, *in press*. [CrossRef]
5. Zhang, N.; Yang, J.; Hu, C. Laser-scribed graphene sensors on nail polish with tunable composition for electrochemical detection of nitrite and glucose. *Sens. Actuators B Chem.* **2022**, *357*, 131394. [CrossRef]
6. Li, Q.; Bai, R.; Gao, Y.; Wu, R.; Ju, K.; Tan, J.; Xuan, F. Laser Direct Writing of Flexible Sensor Arrays Based on Carbonized Carboxymethylcellulose and Its Composites for Simultaneous Mechanical and Thermal Stimuli Detection. *ACS Appl. Mater. Interfaces* **2021**, *13*, 10171–10180. [CrossRef]
7. Nasser, J.; Groo, L.A.; Zhang, L.; Sodano, H. Laser induced graphene fibers for multifunctional aramid fiber reinforced composite. *Carbon* **2020**, *158*, 146–156. [CrossRef]
8. Chyan, Y.; Ye, R.; Li, Y.; Singh, S.P.; Arnusch, C.J.; Tour, J.M. Laser-Induced Graphene by Multiple Lasing: Toward Electronics on Cloth, Paper, and Food. *ACS Nano* **2018**, *12*, 2176–2183. [CrossRef]
9. Kepić, D.; Sandoval, S.; del Pino, P.; György, E.; Cabana, L.; Ballesteros, B.; Tobias, G. Nanosecond Laser-Assisted Nitrogen Doping of Graphene Oxide Dispersions. *ChemPhysChem* **2017**, *18*, 935–941. [CrossRef]
10. Lahcen, A.A.; Rauf, S.; Beduk, T.; Durmus, C.; Aljedaibi, A.; Timur, S.; Alshareef, H.N.; Amine, A.; Wolfbeis, O.S.; Salama, K.N. Electrochemical sensors and biosensors using laser-derived graphene: A comprehensive review. *Biosens. Bioelectron.* **2020**, *168*, 112565. [CrossRef] [PubMed]
11. Liu, J.; Ji, H.; Lv, X.; Zeng, C.; Li, H.; Li, F.; Qu, B.; Cui, F.; Zhou, Q. Laser-induced graphene (LIG)-driven medical sensors for health monitoring and diseases diagnosis. *Microchim. Acta* **2022**, *189*, 54. [CrossRef] [PubMed]
12. Griffiths, K.; Dale, C.; Hedley, J.; Kowal, M.D.; Kaner, R.B.; Keegan, N. Laser-scribed graphene presents an opportunity to print a new generation of disposable electrochemical sensors. *Nanoscale* **2014**, *6*, 13613–13622. [CrossRef]
13. Kavai, M.S.; de Lima, L.F.; de Araujo, W.R. A disposable and low-cost laser-scribed graphene electrochemical sensor for simultaneous detection of hydroquinone, paracetamol and methylparaben. *Mater. Lett.* **2022**, *330*, 133211. [CrossRef]
14. Johnson, Z.T.; Williams, K.; Chen, B.; Sheets, R.; Jared, N.; Li, J.; Smith, E.A.; Claussen, J.C. Electrochemical Sensing of Neonicotinoids Using Laser-Induced Graphene. *ACS Sens.* **2021**, *6*, 3063–3071. [CrossRef]

15. Soares, R.R.A.; Hjort, R.G.; Pola, C.C.; Parate, K.; Reis, E.L.; Soares, N.F.F.; McLamore, E.S.; Claussen, J.C.; Gomes, C.L. Laser-Induced Graphene Electrochemical Immunosensors for Rapid and Label-Free Monitoring of *Salmonella enterica* in Chicken Broth. *ACS Sens.* **2020**, *5*, 1900–1911. [CrossRef] [PubMed]
16. Edberg, J.; Brooke, R.; Hosseinaei, O.; Fall, A.; Wijeratne, K.; Sandberg, M. Laser-induced graphitization of a forest-based ink for use in flexible and printed electronics. *NPJ Flex. Electron.* **2020**, *4*, 17. [CrossRef]
17. Ataide, V.N.; Ameku, W.A.; Bacil, R.P.; Angnes, L.; de Araujo, W.R.; Paixão, T.R.L.C. Enhanced performance of pencil-drawn paper-based electrodes by laser-scribing treatment. *RSC Adv.* **2021**, *11*, 1644–1653. [CrossRef]
18. Wang, A.; Zhu, Y.; Zou, L.; Zhu, H.; Cao, R.; Zhao, G. Combination of machine learning and intelligent sensors in real-time quality control of alcoholic beverages. *Food Sci. Technol.* **2022**, *42*, 1–9. [CrossRef]
19. Beduk, D.; Ilton de Oliveira Filho, J.; Beduk, T.; Harmanci, D.; Zihnioglu, F.; Cicek, C.; Sertoz, R.; Arda, B.; Goksel, T.; Turhan, K.; et al. 'All In One' SARS-CoV-2 variant recognition platform: Machine learning-enabled point of care diagnostics. *Biosens. Bioelectron. X* **2022**, *10*, 100105. [CrossRef]
20. Ha, N.; Xu, K.; Ren, G.; Mitchell, A.; Ou, J.Z. Machine Learning-Enabled Smart Sensor Systems. *Adv. Intell. Syst.* **2020**, *2*, 2000063. [CrossRef]
21. Thamaraiselvan, C.; Wang, J.; James, D.K.; Narkhede, P.; Singh, S.P.; Jassby, D.; Tour, J.M.; Arnusch, C.J. Laser-induced graphene and carbon nanotubes as conductive carbon-based materials in environmental technology. *Mater. Today* **2020**, *34*, 115–131. [CrossRef]
22. Han, T.; Nag, A.; Afsarimanesh, N.; Mukhopadhyay, S.C.; Kundu, S.; Xu, Y. Laser-Assisted Printed Flexible Sensors: A Review. *Sensors* **2019**, *19*, 1462. [CrossRef] [PubMed]
23. Zhao, Y.; Han, Q.; Cheng, Z.; Jiang, L.; Qu, L. Integrated graphene systems by laser irradiation for advanced devices. *Nano Today* **2017**, *12*, 14–30. [CrossRef]
24. Ye, R.; James, D.K.; Tour, J.M. Laser-Induced Graphene: From Discovery to Translation. *Adv. Mater.* **2019**, *31*, e1803621. [CrossRef] [PubMed]
25. Ye, R.; James, D.K.; Tour, J.M. Laser-Induced Graphene. *Acc. Chem. Res.* **2018**, *51*, 1609–1620. [CrossRef]
26. Kurra, N.; Jiang, Q.; Nayak, P.; Alshareef, H.N. Laser-derived graphene: A three-dimensional printed graphene electrode and its emerging applications. *Nano Today* **2019**, *24*, 81–102. [CrossRef]
27. Li, G. Direct laser writing of graphene electrodes. *J. Appl. Phys.* **2020**, *127*, 8725–8729. [CrossRef]
28. Gillani, N.; Arslan, T. Intelligent Sensing Technologies for the Diagnosis, Monitoring and Therapy of Alzheimer's Disease: A Systematic Review. *Sensors* **2021**, *21*, 4249. [CrossRef]
29. Çorman, M.E.; Ozcelikay, G.; Cetinkaya, A.; Kaya, S.I.; Armutcu, C.; Özgür, E.; Uzun, L.; Ozkan, S.A. Metal-organic frameworks as an alternative smart sensing platform for designing molecularly imprinted electrochemical sensors. *TrAC Trends Anal. Chem.* **2022**, *150*, 116573. [CrossRef]
30. Namuduri, S.; Narayanan, B.N.; Davuluru, V.S.P.; Burton, L.; Bhansali, S. Review—Deep Learning Methods for Sensor Based Predictive Maintenance and Future Perspectives for Electrochemical Sensors. *J. Electrochem. Soc.* **2020**, *167*, 037552. [CrossRef]
31. Cui, F.; Yue, Y.; Zhang, Y.; Zhang, Z.; Zhou, H.S. Advancing Biosensors with Machine Learning. *ACS Sens.* **2020**, *5*, 3346–3364. [CrossRef] [PubMed]
32. Beduk, T.; Lahcen, A.A.; Tashkandi, N.; Salama, K.N. One-step electrosynthesized molecularly imprinted polymer on laser scribed graphene bisphenol a sensor. *Sens. Actuators B Chem.* **2020**, *314*, 128026. [CrossRef]
33. Wan, Z.; Umer, M.; Lobino, M.; Thiel, D.; Nguyen, N.-T.; Trinchi, A.; Shiddiky, M.J.A.; Gao, Y.; Li, Q. Laser induced self-N-doped porous graphene as an electrochemical biosensor for femtomolar miRNA detection. *Carbon* **2020**, *163*, 385–394. [CrossRef]
34. Lei, Y.; Alshareef, A.H.; Zhao, W.; Inal, S. Laser-Scribed Graphene Electrodes Derived from Lignin for Biochemical Sensing. *ACS Appl. Nano Mater.* **2020**, *3*, 1166–1174. [CrossRef]
35. Zhao, G.; Wang, F.; Zhang, Y.; Sui, Y.; Liu, P.; Zhang, Z.; Xu, C.; Yang, C. High-performance hydrogen peroxide micro-sensors based on laser-induced fabrication of graphene@Ag electrodes. *Appl. Surf. Sci.* **2021**, *565*, 150565. [CrossRef]
36. Ghanam, A.; Lahcen, A.A.; Beduk, T.; Alshareef, H.N.; Amine, A.; Salama, K.N. Laser scribed graphene: A novel platform for highly sensitive detection of electroactive biomolecules. *Biosens. Bioelectron.* **2020**, *168*, 112509. [CrossRef]
37. Rocha, D.P.; Ataide, V.N.; de Siervo, A.; Gonçalves, J.M.; Muñoz, R.A.; Paixão, T.R.; Angnes, L. Reagentless and sub-minute laser-scribing treatment to produce enhanced disposable electrochemical sensors via additive manufacture. *Chem. Eng. J.* **2021**, *425*, 130594. [CrossRef]
38. Mendes, L.F.; de Siervo, A.; de Araujo, W.R.; Paixão, T.R.L.C. Reagentless fabrication of a porous graphene-like electrochemical device from phenolic paper using laser-scribing. *Carbon* **2020**, *159*, 110–118. [CrossRef]
39. Zhang, Z.; Song, M.; Hao, J.; Wu, K.; Li, C.; Hu, C. Visible light laser-induced graphene from phenolic resin: A new approach for directly writing graphene-based electrochemical devices on various substrates. *Carbon* **2018**, *127*, 287–296. [CrossRef]
40. Kothuru, A.; Goel, S. Laser induced graphene on phenolic resin and alcohol composite sheet for flexible electronics applications. *Flex. Print. Electron.* **2020**, *5*, 042001. [CrossRef]
41. Liu, J.; Zhang, L.; Yang, C.; Tao, S. Preparation of multifunctional porous carbon electrodes through direct laser writing on a phenolic resin film. *J. Mater. Chem. A* **2019**, *7*, 21168–21175. [CrossRef]

42. Loguercio, L.F.; Thesing, A.; Noremberg, B.D.S.; Lopes, B.V.; Maron, G.K.; Machado, G.; Pope, M.A.; Carreno, N.L.V. Direct Laser Writing of Poly(furfuryl Alcohol)/Graphene Oxide Electrodes for Electrochemical Determination of Ascorbic Acid. *ChemElectroChem* **2022**, *9*, e202200334. [CrossRef]
43. Yuan, X.; Chen, J.; Ling, Y.; Yu, S.; Li, S.; Wu, X.; Zhang, Z. A facile and efficient nitrite electrochemical sensor based on N, O co-doped porous graphene film. *Microchem. J.* **2022**, *178*, 107361. [CrossRef]
44. Nasraoui, S.; Al-Hamry, A.; Teixeira, P.R.; Ameur, S.; Paterno, L.G.; Ben Ali, M.; Kanoun, O. Electrochemical sensor for nitrite detection in water samples using flexible laser-induced graphene electrodes functionalized by CNT decorated by Au nanoparticles. *J. Electroanal. Chem.* **2021**, *880*, 114893. [CrossRef]
45. Sharma, S.; Ganeshan, S.K.; Pattnaik, P.K.; Kanungo, S.; Chappanda, K.N. Laser induced flexible graphene electrodes for electrochemical sensing of hydrazine. *Mater. Lett.* **2020**, *262*, 127150. [CrossRef]
46. Xu, Z.; Fan, X.; Ma, Q.; Tang, B.; Lu, Z.; Zhang, J.; Mo, G.; Ye, J.; Ye, J. A sensitive electrochemical sensor for simultaneous voltammetric sensing of cadmium and lead based on Fe3O4/multiwalled carbon nanotube/laser scribed graphene composites functionalized with chitosan modified electrode. *Mater. Chem. Phys.* **2019**, *238*, 121877. [CrossRef]
47. Zhu, Y.; Liu, P.; Xue, T.; Xu, J.; Qiu, D.; Sheng, Y.; Li, W.; Lu, X.; Ge, Y.; Wen, Y. Facile and rapid one-step mass production of flexible 3D porous graphene nanozyme electrode via direct laser-writing for intelligent evaluation of fish freshness. *Microchem. J.* **2021**, *162*, 105855. [CrossRef]
48. Zeng, Y.; Li, Q.; Wang, W.; Wen, Y.; Ji, K.; Liu, X.; He, P.; Janegitz, B.C.; Tang, K. The fabrication of a flexible and portable sensor based on home-made laser-induced porous graphene electrode for the rapid detection of sulfonamides. *Microchem. J.* **2022**, *182*, 107898. [CrossRef]
49. Lin, X.; Lu, Z.; Zhang, Y.; Liu, B.; Mo, G.; Li, J.; Ye, J. A glassy carbon electrode modified with a bismuth film and laser etched graphene for simultaneous voltammetric sensing of Cd(II) and Pb(II). *Microchim. Acta* **2018**, *185*, 438. [CrossRef]
50. Rajaji, U.; Govindasamy, M.; Sha, R.; Alshgari, R.A.; Juang, R.-S.; Liu, T.-Y. Surface engineering of 3D spinel Zn3V2O8 wrapped on sulfur doped graphitic nitride composites: Investigation on the dual role of electrocatalyst for simultaneous detection of antibiotic drugs in biological fluids. *Compos. Part B Eng.* **2022**, *242*, 110017. [CrossRef]
51. You, Z.; Qiu, Q.; Chen, H.; Feng, Y.; Wang, X.; Wang, Y.; Ying, Y. Laser-induced noble metal nanoparticle-graphene composites enabled flexible biosensor for pathogen detection. *Biosens. Bioelectron.* **2020**, *150*, 111896. [CrossRef] [PubMed]
52. Rajaji, U.; Ganesh, P.-S.; Kim, S.-Y.; Govindasamy, M.; Alshgari, R.A.; Liu, T.-Y. MoS_2 Sphere/2D S-Ti_3C_2 MXene Nanocatalysts on Laser-Induced Graphene Electrodes for Hazardous Aristolochic Acid and Roxarsone Electrochemical Detection. *ACS Appl. Nano Mater.* **2022**, *5*, 3252–3264. [CrossRef]
53. Ge, L.; Guo, C.; Li, H.; Xia, X.; Chen, L.; Ning, D.; Liu, X.; Li, F. Direct-laser-writing of electrochemiluminescent electrode on glassy carbon for iodide sensing in aqueous solution. *Sens. Actuators B Chem.* **2021**, *337*, 129766. [CrossRef]
54. Lin, X.; Lu, Z.; Dai, W.; Liu, B.; Zhang, Y.; Li, J.; Ye, J. Laser engraved nitrogen-doped graphene sensor for the simultaneous determination of Cd(II) and Pb(II). *J. Electroanal. Chem.* **2018**, *828*, 41–49. [CrossRef]
55. Nayak, P.; Kurra, N.; Xia, C.; Alshareef, H.N. Highly Efficient Laser Scribed Graphene Electrodes for On-Chip Electrochemical Sensing Applications. *Adv. Electron. Mater.* **2016**, *2*, 1600185. [CrossRef]
56. Xu, G.; Jarjes, Z.A.; Desprez, V.; Kilmartin, P.A.; Travas-Sejdic, J. Sensitive, selective, disposable electrochemical dopamine sensor based on PEDOT-modified laser scribed graphene. *Biosens. Bioelectron.* **2018**, *107*, 184–191. [CrossRef] [PubMed]
57. Xu, L.; Wu, R.; Zhu, X.; Wang, X.; Geng, X.; Xiong, Y.; Chen, T.; Wen, Y.; Ai, S. Intelligent analysis of maleic hydrazide using a simple electrochemical sensor coupled with machine learning. *Anal. Methods* **2021**, *13*, 4662–4673. [CrossRef]
58. Li, D.; Shao, Y.; Zhang, Q.; Qu, M.; Ping, J.; Fu, Y.; Xie, J. A flexible virtual sensor array based on laser-induced graphene and MXene for detecting volatile organic compounds in human breath. *Analyst* **2021**, *146*, 5704–5713. [CrossRef]
59. Zhu, X.; Lin, L.; Wu, R.; Zhu, Y.; Sheng, Y.; Nie, P.; Liu, P.; Xu, L.; Wen, Y. Portable wireless intelligent sensing of ultra-trace phytoregulator α-naphthalene acetic acid using self-assembled phosphorene/Ti3C2-MXene nanohybrid with high ambient stability on laser induced porous graphene as nanozyme flexible electrode. *Biosens. Bioelectron.* **2021**, *179*, 113062. [CrossRef]
60. Li, M.; Zhou, P.; Wang, X.; Wen, Y.; Xu, L.; Hu, J.; Huang, Z.; Li, M. Development of a simple disposable laser-induced porous graphene flexible electrode for portable wireless intelligent votammetric nanosensing of salicylic acid in agro-products. *Comput. Electron. Agric.* **2021**, *191*, 106502. [CrossRef]
61. Getachew, B.A.; Bergsman, D.S.; Grossman, J.C. Laser-Induced Graphene from Polyimide and Polyethersulfone Precursors as a Sensing Electrode in Anodic Stripping Voltammetry. *ACS Appl. Mater. Interfaces* **2020**, *12*, 48511–48517. [CrossRef] [PubMed]
62. Liu, Y.; Xue, Q.; Chang, C.; Wang, R.; Wang, Q.; Shan, X. Highly efficient detection of Cd(II) ions by a stannum and cerium bimetal-modified laser-induced graphene electrode in water. *Chem. Eng. J.* **2022**, *433*, 133791. [CrossRef]
63. Samoson, K.; Soleh, A.; Saisahas, K.; Promsuwan, K.; Saichanapan, J.; Kanatharana, P.; Thavarungkul, P.; Chang, K.H.; Abdullah, A.F.L.; Tayayuth, K.; et al. Facile fabrication of a flexible laser induced gold nanoparticle/chitosan/ porous graphene electrode for uric acid detection. *Talanta* **2022**, *243*, 123319. [CrossRef] [PubMed]
64. Kammarchedu, V.; Butler, D.; Ebrahimi, A. A machine learning-based multimodal electrochemical analytical device based on eMoSx-LIG for multiplexed detection of tyrosine and uric acid in sweat and saliva. *Anal. Chim. Acta* **2022**, *1232*, 340447. [CrossRef] [PubMed]

65. Madhuvilakku, R.; Yen, Y.-K.; Yan, W.-M.; Huang, G.-W. Laser-scribed Graphene Electrodes Functionalized with Nafion/Fe_3O_4 Nanohybrids for the Ultrasensitive Detection of Neurotoxin Drug Clioquinol. *ACS Omega* **2022**, *7*, 15936–15950. [CrossRef] [PubMed]
66. Fenzl, C.; Nayak, P.; Hirsch, T.; Wolfbeis, O.S.; Alshareef, H.N.; Baeumner, A.J. Laser-Scribed Graphene Electrodes for Aptamer-Based Biosensing. *ACS Sens.* **2017**, *2*, 616–620. [CrossRef]
67. Liu, X.; Cheng, H.; Zhao, Y.; Wang, Y.; Li, F. Portable electrochemical biosensor based on laser-induced graphene and MnO2 switch-bridged DNA signal amplification for sensitive detection of pesticide. *Biosens. Bioelectron.* **2022**, *199*, 113906. [CrossRef]
68. Zhao, J.; Zheng, C.; Gao, J.; Gui, J.; Deng, L.; Wang, Y.; Xu, R. Co3O4 nanoparticles embedded in laser-induced graphene for a flexible and highly sensitive enzyme-free glucose biosensor. *Sens. Actuators B Chem.* **2021**, *347*, 130653. [CrossRef]
69. Zhang, L.; Wang, L.; Li, J.; Cui, C.; Zhou, Z.; Wen, L. Surface Engineering of Laser-Induced Graphene Enables Long-Term Monitoring of On-Body Uric Acid and pH Simultaneously. *Nano Lett.* **2022**, *22*, 5451–5458. [CrossRef]
70. Rossato, J.H.H.; Oliveira, M.E.; Lopes, B.V.; Gallo, B.B.; La Rosa, A.B.; Piva, E.; Barba, D.; Rosei, F.; Carreño, N.L.V.; Escote, M.T. A Flexible Electrochemical Biosensor Based on $NdNiO_3$ Nanotubes for Ascorbic Acid Detection. *ACS Appl. Nano Mater.* **2022**, *5*, 3394–3405. [CrossRef]
71. Barman, S.C.; Zahed, M.A.; Sharifuzzaman, M.; Ko, S.G.; Yoon, H.; Nah, J.S.; Xuan, X.; Park, J.Y. A Polyallylamine Anchored Amine-Rich Laser-Ablated Graphene Platform for Facile and Highly Selective Electrochemical IgG Biomarker Detection. *Adv. Funct. Mater.* **2020**, *30*, 1907297. [CrossRef]
72. Johnson, Z.T.; Jared, N.; Peterson, J.K.; Li, J.; Smith, E.A.; Walper, S.A.; Hooe, S.L.; Breger, J.C.; Medintz, I.L.; Gomes, C.; et al. Enzymatic Laser-Induced Graphene Biosensor for Electrochemical Sensing of the Herbicide Glyphosate. *Glob. Chall.* **2022**, *6*, 2200057. [CrossRef] [PubMed]
73. Liao, J.; Zhang, X.; Sun, Z.; Chen, H.; Fu, J.; Si, H.; Ge, C.; Lin, S. Laser-Induced Graphene-Based Wearable Epidermal Ion-Selective Sensors for Noninvasive Multiplexed Sweat Analysis. *Biosensors* **2022**, *12*, 397. [CrossRef] [PubMed]
74. Arantes, I.V.S.; Paixão, T.R.L.C. Couple batch-injection analysis and microfluidic paper-based analytical device: A simple and disposable alternative to conventional BIA apparatus. *Talanta* **2022**, *240*, 123201. [CrossRef] [PubMed]
75. Hui, X.; Xuan, X.; Kim, J.; Park, J.Y. A highly flexible and selective dopamine sensor based on Pt-Au nanoparticle-modified laser-induced graphene. *Electrochimica Acta* **2019**, *328*, 135066. [CrossRef]
76. Wang, G.; Chen, J.; Huang, L.; Chen, Y.; Li, Y. A laser-induced graphene electrochemical immunosensor for label-free CEA monitoring in serum. *Analyst* **2021**, *146*, 6631–6642. [CrossRef]
77. Beduk, T.; Beduk, D.; de Oliveira Filho, J.I.; Zihnioglu, F.; Cicek, C.; Sertoz, R.; Arda, B.; Goksel, T.; Turhan, K.; Salama, K.N.; et al. Rapid Point-of-Care COVID-19 Diagnosis with a Gold-Nanoarchitecture-Assisted Laser-Scribed Graphene Biosensor. *Anal. Chem.* **2021**, *93*, 8585–8594. [CrossRef]
78. Torrente-Rodríguez, R.M.; Lukas, H.; Tu, J.; Min, J.; Yang, Y.; Xu, C.; Rossiter, H.B.; Gao, W. SARS-CoV-2 RapidPlex: A Graphene-Based Multiplexed Telemedicine Platform for Rapid and Low-Cost COVID-19 Diagnosis and Monitoring. *Matter* **2020**, *3*, 1981–1998. [CrossRef]
79. Puthongkham, P.; Wirojsaengthong, S.; Suea-Ngam, A. Machine learning and chemometrics for electrochemical sensors: Moving forward to the future of analytical chemistry. *Analyst* **2021**, *146*, 6351–6364. [CrossRef]
80. Zhu, X.; Liu, P.; Xue, T.; Ge, Y.; Ai, S.; Sheng, Y.; Wu, R.; Xu, L.; Tang, K.; Wen, Y. A novel graphene-like titanium carbide MXene/Au–Ag nanoshuttles bifunctional nanosensor for electrochemical and SERS intelligent analysis of ultra-trace carbendazim coupled with machine learning. *Ceram. Int.* **2021**, *47*, 173–184. [CrossRef]
81. Fang, L.; Liao, X.; Jia, B.; Shi, L.; Kang, L.; Zhou, L.; Kong, W. Recent progress in immunosensors for pesticides. *Biosens. Bioelectron.* **2020**, *164*, 112255. [CrossRef] [PubMed]
82. Warra, A.A.; Prasad, M.N.V. African perspective of chemical usage in agriculture and horticulture—Their impact on human health and environment. In *Agrochemicals Detection, Treatment and Remediation*; Butterworth-Heinemann: Oxford, UK, 2020; pp. 401–436, ISBN 9780081030172.
83. Sharma, A.; Shukla, A.; Attri, K.; Kumar, M.; Kumar, P.; Suttee, A.; Singh, G.; Barnwal, R.P.; Singla, N. Global trends in pesticides: A looming threat and viable alternatives. *Ecotoxicol. Environ. Saf.* **2020**, *201*, 110812. [CrossRef] [PubMed]
84. Cao, J.; Wang, M.; Yu, H.; She, Y.; Cao, Z.; Ye, J.; El-Aty, A.M.A.; Hacimuftuoglu, A.; Wang, J.; Lao, S. An Overview on the Mechanisms and Applications of Enzyme Inhibition-Based Methods for Determination of Organophosphate and Carbamate Pesticides. *J. Agric. Food Chem.* **2020**, *68*, 7298–7315. [CrossRef] [PubMed]
85. Parra-Arroyo, L.; González-González, R.B.; Castillo-Zacarías, C.; Melchor Martínez, E.M.; Sosa-Hernández, J.E.; Bilal, M.; Iqbal, H.M.N.; Barceló, D.; Parra-Saldívar, R. Highly hazardous pesticides and related pollutants: Toxicological, regulatory, and analytical aspects. *Sci. Total Environ.* **2022**, *807*, 18–26. [CrossRef] [PubMed]
86. Andersson, E.; Persson, S.; Hallén, N.; Ericsson, Å.; Thielke, D.; Lindgren, P.; Carlsson, K.S.; Jendle, J. Costs of diabetes complications: Hospital-based care and absence from work for 392,200 people with type 2 diabetes and matched control participants in Sweden. *Diabetologia* **2020**, *63*, 2582–2594. [CrossRef] [PubMed]
87. Speth, J.D. Neanderthals, vitamin C., and scurvy. *Quat. Int.* **2018**, *500*, 172–184. [CrossRef]
88. Zhang, S.; Song, Y.; Wang, M.; Xiao, G.; Gao, F.; Li, Z.; Tao, G.; Zhuang, P.; Yue, F.; Chan, P.; et al. Real-time simultaneous recording of electrophysiological activities and dopamine overflow in the deep brain nuclei of a non-human primate with Parkinson's disease using nano-based microelectrode arrays. *Microsyst. Nanoeng.* **2018**, *4*, 17070. [CrossRef]

89. Alba, A.F.; Totoricaguena-Gorriño, J.; Sánchez-Ilárduya, M.B.; Ruiz-Rubio, L.; Vilas-Vilela, J.L.; Lanceros-Méndez, S.; del Campo, F.J. Laser-activated screen-printed carbon electrodes for enhanced dopamine determination in the presence of ascorbic and uric acid. *Electrochim. Acta* **2021**, *399*, 139374. [CrossRef]
90. Zarenezhad, E.; Farjam, M.; Iraji, A. Synthesis and biological activity of pyrimidines-containing hybrids: Focusing on pharmacological application. *J. Mol. Struct.* **2021**, *1230*, 129833. [CrossRef]
91. Xing, L.; Zhang, W.; Fu, L.; Lorenzo, J.M.; Hao, Y. Fabrication and application of electrochemical sensor for analyzing hydrogen peroxide in food system and biological samples. *Food Chem.* **2022**, *385*, 132555. [CrossRef]
92. Liu, Y.; Nguyen, M.; Robert, A.; Meunier, B. Metal Ions in Alzheimer's Disease: A Key Role or Not? *Acc. Chem. Res.* **2019**, *52*, 2026–2035. [CrossRef] [PubMed]
93. Megha, K.B.; Mohanan, P.V. Role of immunoglobulin and antibodies in disease management. *Int. J. Biol. Macromol.* **2021**, *169*, 28–38. [CrossRef] [PubMed]
94. Luyendyk, J.P.; Schoenecker, J.G.; Flick, M.J. The multifaceted role of fibrinogen in tissue injury and inflammation. *Blood* **2019**, *133*, 511–520. [CrossRef] [PubMed]
95. Gourama, H. Foodborne Pathogens. In *Food Safety Engineering*; Demirci, A., Feng, H., Krishnamurthy, K., Eds.; Springer International Publishing: Cham, Germany, 2020; pp. 25–49, ISBN 978-3-030-42660-6.
96. Mutalik, V.K.; Adler, B.A.; Rishi, H.S.; Piya, D.; Zhong, C.; Koskella, B.; Kutter, E.M.; Calendar, R.; Novichkov, P.S.; Price, M.N.; et al. High-throughput mapping of the phage resistance landscape in *E. coli*. *PLoS Biol.* **2020**, *18*, e3000877. [CrossRef]